Detecting and mapping leafy spurge (Euphorbia esula) and spotted knapweed (Centaurea maculosa) in rangeland ecosystems using airborne digital imagery
by Shana Grace Driscoll

A thesis submitted in partial fulfillment of the requirements for the degree of Master of Science in Land Resources and Environmental Sciences
Montana State University

Abstract:
Invasive nonindigenous plants are threatening the biological integrity of North American rangelands, as well as the economies that are supported by those ecosystems. To reduce the rapid spread of invasive plants, management strategies should focus on early detection, prevention, and eradication. Spatial information is critical to fulfilling invasive plant management strategies. Traditional invasive plant mapping has utilized ground-based hand or GPS mapping. The shortfalls of ground-based methods include the limited spatial extent covered and the associated time and cost. Mapping vegetation with remote sensing covers large spatial areas and maps can be updated at an interval determined by management needs.

The objectives of the study were to classify (1) 4-band multispectral (1 m resolution) and 128-band hyperspectral (5 m and 3 m resolution) imagery for Euphorbia esula and Centaurea maculosa, (2) to assess the accuracy of the classifications, and (3) to compare accuracy assessments for multispectral and hyperspectral classifications using Kappa analysis.

Ground reference samples were collected to extract image statistics for classification algorithms and to perform accuracy assessments. A maximum likelihood (ML) classification algorithm was applied to the multispectral imagery. Spectral angle mapper (SAM) and classification and regression tree (CART) analysis were applied to the hyperspectral imagery. Confusion matrices for each classification were generated and summary measures were calculated.

Color balancing was applied to the multispectral imagery and compared to non-color balanced imagery to test the effect on classification accuracy. There were no significant differences between Khat statistics for color balanced multispectral imagery and noncolor balanced multispectral imagery for both target species.

Summary measures (overall, user's, and producer's accuracies, and Khat statistic) were higher for the hyperspectral CART classification than for the multispectral ML classification for both target species. Khat statistics for the hyperspectral CART and SAM classifications were not significantly different for E. esula, however for C. maculosa the CART algorithm showed significant improvement over SAM. User's accuracies for the hyperspectral CART classifications for both target species were within moderate ground-based mapping accuracy levels. Such remote mapping methodologies have shown utility for estimating distribution of these invasive plants over large areas.

DETECTING AND MAPPING LEAFY SPURGE (*EUPHORBIA ESULA*) AND SPOTTED KNAPWEED (*CENTAUREA MACULOSA*) IN RANGELAND ECOSYSTEMS USING AIRBORNE DIGITAL IMAGERY

by

Shana Grace Driscoll

A thesis submitted in partial fulfillment
of the requirements for the degree

of

Master of Science

in

Land Resources and Environmental Sciences

MONTANA STATE UNIVERSITY
Bozeman, Montana

April 2002

APPROVAL

Of a thesis submitted by

Shana Grace Driscoll

This thesis has been read by each member of the thesis committee and has been found to be satisfactory regarding content, English usage, format, citations, bibliographic style, and consistency, and is ready for submission to the College of Graduate Studies.

Rick L. Lawrence ______________________ 4/16/02
Date

Roger L. Sheley ______________________ 4/17/02
Date

Approved for the Department of Land Resources and Environmental Sciences

Jeffrey S. Jacobsen ______________________ 4/17/02
Date

Approved for the College of Graduate Studies

Bruce R. McLeod ______________________ 4-19-02
Date

STATEMENT OF PERMISSION TO USE

In presenting this thesis in partial fulfillment of the requirements for a master's degree at Montana State University, I agree that the Library shall make it available to borrowers under rules of the Library.

If I have indicated my intention to copyright this thesis by including a copyright notice page, copying is allowable only for scholarly purposes, consistent with "fair use" as prescribed in the U. S. Copyright Law. Requests for permission for extended quotation from or reproduction of this thesis in whole or in parts may be granted only by the copyright holder.

Signature Shana V Driscoll

Date 4/17/02

ACKNOWLEDGEMENTS

I wish to express gratitude to Rick Lawrence and Roger Sheley for their patience and support in guiding me through the tremendous learning experience that comprises master's level study. Their doors were always open and their ideas always shared with enthusiasm. Thank you also to Richard Aspinall for his spatial and statistical insight given at critical moments. I deeply appreciate the invaluable skills and tools given by all.

I am grateful to the Montana Noxious Weed Trust Fund for the generous funding that allowed me to pursue the mapping project.

And thank you to Ted Wood for bringing me good coffee in the morning.

TABLE OF CONTENTS

TABLE OF CONTENTS - Continued

TABLE OF CONTENTS - Continued

LIST OF TABLES

LIST OF TABLES - Continued

LIST OF FIGURES

ABSTRACT

Invasive nonindigenous plants are threatening the biological integrity of North American rangelands, as well as the economies that are supported by those ecosystems. To reduce the rapid spread of invasive plants, management strategies should focus on early detection, prevention, and eradication. Spatial information is critical to fulfilling invasive plant management strategies. Traditional invasive plant mapping has utilized ground-based hand or GPS mapping. The shortfalls of ground-based methods include the limited spatial extent covered and the associated time and cost. Mapping vegetation with remote sensing covers large spatial areas and maps can be updated at an interval determined by management needs.

The objectives of the study were to classify (1) 4-band multispectral (1 m resolution) and 128-band hyperspectral (5 m and 3 m resolution) imagery for *Euphorbia esula* and *Centaurea maculosa*, (2) to assess the accuracy of the classifications, and (3) to compare accuracy assessments for multispectral and hyperspectral classifications using Kappa analysis.

Ground reference samples were collected to extract image statistics for classification algorithms and to perform accuracy assessments. A maximum likelihood (ML) classification algorithm was applied to the multispectral imagery. Spectral angle mapper (SAM) and classification and regression tree (CART) analysis were applied to the hyperspectral imagery. Confusion matrices for each classification were generated and summary measures were calculated.

Color balancing was applied to the multispectral imagery and compared to non-color balanced imagery to test the effect on classification accuracy. There were no significant differences between Khat statistics for color balanced multispectral imagery and non-color balanced multispectral imagery for both target species.

Summary measures (overall, user's, and producer's accuracies, and Khat statistic) were higher for the hyperspectral CART classification than for the multispectral ML classification for both target species. Khat statistics for the hyperspectral CART and SAM classifications were not significantly different for *E. esula*, however for *C. maculosa* the CART algorithm showed significant improvement over SAM. User's accuracies for the hyperspectral CART classifications for both target species were within moderate ground-based mapping accuracy levels. Such remote mapping methodologies have shown utility for estimating distribution of these invasive plants over large areas.

CHAPTER 1

INTRODUCTION

Invasive Plant Management: Mapping Strategies

Invasive non-indigenous plants are negatively impacting the biology and ecology of North American rangelands (Sheley et al. 1996, Vitousek et al. 1996), as well as the economies that are supported by those rangeland ecosystems (Bangsund et al. 1993, Bangsund et al. 1999). Invasive plant management plans designed to detect, prevent dispersal of, and eradicate invasive species provide an organized and strategic approach to minimizing ecologic and economic impacts of noxious weed infestations (Johnson 1999). To design and implement effective invasive plant management plans, accurate and updated location information about weed distributions is essential (Anderson et al. 1996). One important strategy of successful weed management is detecting small weed infestations before they grow too large to control feasibly (Moody and Mack 1988, Zamora and Thill 1999). In addition, repeated monitoring and mapping of areas in which distributions have changed can guide managers in assessing the effectiveness of weed prevention and control measures (Cooksey and Sheley 1998b). Mapping methods that utilize the resolution required to identify small, localized populations of invasive weeds, yet are efficient and practical enough to repeat on short temporal scales and apply to landscape scales will promote effective management of invasive plants in rangeland ecosystems (Johnson 1999). Throughout this study, the use of "landscape scale" refers to large geographical areas that have a common land management goal, for example county weed management areas, or state/federal wildlife reserves, grazing allotments, and wild and scenic river corridors.

Ground-Based Mapping

Invasive plant management plans have traditionally utilized maps created by field survey to delineate plant infestations onto paper maps or more recently by using global positioning system (GPS) technology to create a digital geographic database (Cooksey and Sheley 1997). Field mapping is most often performed on the ground and, at greater monetary expense, can be achieved through aerial (fixed wing or helicopter) survey. Systematic, intensive ground-based mapping over large spatial extents however, is hindered by financial and logistical constraints because of the limited spatial extent that can be feasibly covered by ground-based mapping. The Montana Noxious Weed Survey and Mapping System developed standardized guidelines and methods for inventorying and mapping invasive plants, as well as levels of accuracy for hand and GPS mapping (Cooksey and Sheley 1998a). Level I accuracy, defined as having attribute accuracy of 80 – 100% and horizontal accuracy of 0 – 20 m (Cooksey and Sheley 1998a), was estimated to cost between $3 – 5 per acre (Mullin 2000). The costs of collecting high accuracy data might impede follow-up mapping. To our knowledge, an appropriate interval for updating invasive plant maps has not been described, and update frequency might be most appropriately defined by specific invasive plant or site management objectives. Invasive plant maps should be updated on time scales that allow managers to monitor and assess effectiveness of management plans based on the dynamic nature of weed populations and the landscapes they invade.

Remote Mapping

Mapping vegetation from airborne or satellite platforms can encompass large geographical extents (Ioka and Koda 1986, Treitz et al. 1992, Ustin et al. 1996, Lauver 1997, Roberts et al. 1998), and if operationally efficient methods for weed mapping are developed and proven, then remote sensing might have the potential to be more time and cost efficient than ground mapping. The savings in time and cost on the ground could allow managers to invest in repeated inventory and mapping, thus updating their weed distribution maps as needed. For example, in Theodore Roosevelt National Park (TRNP), maps derived from aerial photography were used to develop a park-wide comprehensive leafy spurge management plan (Anderson et al. 1996). The impact of management was assessed several years later when TRNP was mapped again using the Airborne Visible Infrared Imaging Spectrometer. Managers at TRNP used the updated maps to assess the impact of biocontrol and other management tools (Root et al. 2001). Most managers, however, have not used digital remote sensing to assist in developing and implementing invasive plant management plans because of coarse resolution imagery and high costs (Johnson 1999). In addition, until the 1990s remotely sensed map accuracies were rarely quantified (Congalton 1991), and so fitness for a particular management goal could not be assessed.

Over the past decade, detecting and mapping invasive plant populations using remote sensing has received more attention from a research and development perspective in government and academia (Peters et al. 1992, Everitt et al. 1995b, Lass and Callihan 1997, Root et al. 2001). Commercial sensors have been developed with increased spatial and spectral resolution compared to traditional sensors such as the National Aeronautics and Space Administration's Landsat sensors, the National Oceanic and Atmospheric Administration's Advanced Very High Resolution Radiometer, and conventional film-based cameras used in aerial photography (Coulter et al. 2000, Lefsky et al. 2001). If practical, efficient, and inexpensive techniques for mapping weeds can be developed, these higher resolution, commercially available sensors might provide the accuracy and cost-competitiveness to enable landscape-scale weed mapping.

Objectives

The overall objective of this study was to map *Euphorbia esula* L. (leafy spurge) and *Centaurea maculosa* Lam. (spotted knapweed) by classifying two commercially available types of airborne digital imagery and quantifying and comparing the resulting map accuracies. In the interest of employing methods that were operationally practical and user-oriented, I used classification algorithms embedded in commercially available image processing and statistical software.

I provide a review of research and literature pertinent to remote sensing as a tool for mapping vegetation, with particular focus on invasive plant species, in Chapter 2. In Chapter 3, which is written for publication, I present methods used to process and classify the imagery and compare accuracy assessments for the resulting invasive plant maps. The accuracy assessments presented in Chapter 3 are twofold: one method is based on hard interpretation of polygon membership; the other is based on interpretation of polygon membership with incremental percentage thresholds. In addition, multispectral and hyperspectral imagery are compared in Chapter 3. Chapter 4 was written as a technical paper to be presented at a professional conference. In Chapter 4, I test methods for correcting illumination variations inherent to airborne imagery and compare the results of color balancing to no color balancing on classification accuracy. I summarize the effectiveness of the methodology with respect to ground-based mapping and implications of remote mapping for invasive plant management in Chapter 5.

CHAPTER 2

LITERATURE REVIEW

Introduction

Monitoring vegetation distribution, composition, and function is a primary goal of applied ecology (Sheley et al. 1996, O'Neill et al. 1997, Gould 2000). Such goals will become more important as scientists continue to address the impacts to plant communities from global and regional climate change, changes in land use practices, and invasion of nonindigenous plant species. The need for spanning wide spatial and temporal scales is integral to understanding the full impact of dynamic ecological processes because disturbances are often unconstrained by environmental boundaries or gradients and affect both global and local systems (Graetz 1989, Caldow and Racey 2000). Further, landscape scale studies of vegetation dynamics provide information to support resource management and conservation decision-making processes (Tueller 1989, Lauver 1997, Wessman et al. 1997, Coulter et al. 2000, Price et al. 2001). Remote sensing has developed into a powerful tool for measuring and monitoring vegetation characteristics over large areas (O'Neill et al. 1997) and with high temporal resolution (Hobbs 1989).

Land cover mapping has long been a use of remote sensing (Anderson et al. 1976), and correlations between reflectance and green biomass have been used to map vegetation communities at global scales (Tucker et al. 1985). Extracting specific information about vegetation composition or type remotely has not met with the same success (Graetz 1989), and research into improving remote mapping at the species level is continually advancing (Lees and Ritman 1991, Ustin et al. 1996, Lewis 1998, Martin et al. 1998, Roberts et al. 1998). The purpose of this chapter is to discuss issues related to mapping vegetation remotely including plant reflectance characteristics, bidirectional reflectance, resolution, classification algorithms, and accuracy assessment.

Reflectance Characteristics of Vegetation

While remote identification and mapping of minerals has been relatively successful (Kruse 1988, Kruse et al. 1999), vegetation offers a greater challenge because of the similar composition of photosynthesizing plants and complex interactions at the plant surface (Cochrane 2000). In general, most green plants absorb and reflect light in a similar manner because they are composed of the same chemical constituents including chlorophylls, carotenoids and other pigments, cellulose, and lignin (Knipling 1970). Studies of leaf reflectance in the 1960s have characterized well the interaction of vegetation with light (Gates et al. 1965, Knipling 1970). Pigments, including chlorophyll, absorb visible light (Gates et al. 1965, Knipling 1970, Woolley 1971, Gausman 1977). The amount of water contained in plant tissue affects reflectance at all wavelengths. Water infiltrating the spaces between cell walls has a higher refractive index than air, causing greater absorption in both the visible and near-infrared range (Woolley 1971). Cellular architecture within the mesophyll of a leaf causes a sharp increase in reflectance in the near-infrared range (Gausman 1977). Early senescence causes an increase in reflectance as more air cavities are created with shrinking and splitting cells; however, as cells deteriorate fully in late senescence reflectance decreases significantly (Knipling 1970).

Structure and morphology also determine how plants reflect light (Knipling 1970, Woolley 1971). Plants with pubescent leaves were found to have higher visible reflectance than glabrous-leaved plants, and discriminant analysis of field and spectral variables found that reflectance at 450, 650, and 850 nm combined with plant height explained the greatest variability in leaf pubescence (Everitt and Richerson 1987). Structural characteristics (height) of the grass species *Spartina foliosa* Trin. (California cordgrass) were estimated with airborne digital imagery in a restored salt marsh in San Diego County, California (Phinn et al. 1999). Unique coloration of vegetation, particularly when flowering, has also been used to discriminate between species using aerial photography and videography. Researchers detected and mapped *Tamarix chinensis* Lour. (tamarisk) from associated vegetation and soil after senescence when the plant exhibited a distinct orange-yellow color (Everitt and Deloach 1990, Everitt et al. 1996). In addition, researchers found that *Isocoma drummondii* (T.&G.) Greene (Drummond goldenweed) differed significantly from associated vegetation during the bright golden flowering period and they used the high visible reflectance to classify aerial photographs for plant quantities (Everitt et al. 1992).

Although identifying vegetation to the taxonomic level has been called the "difficult third dimension" of remotely based vegetation studies (Graetz 1989), the importance of mapping species composition and diversity is expanding and methods for doing so are struggling to keep pace with the need (Lauver 1997, Gould 2000). While structure and morphology have provided unique traits that allow for remote identification, these same characteristics often enhance the variability with which vegetation reflects incoming solar radiance, making it difficult to spectrally separate plant species (Sandmeier et al. 1998).

Bidirectional Reflectance

Bidirectional reflectance of a scene results from the interaction of viewing (sensor) direction and illumination (sun) position (Norman et al. 1985, Lillesand and Kiefer 2000). Bidirectional reflectance exhibits spatial dependence because sun-sensor geometry changes slightly with each ground cell imaged (Foody 1988). As a result, dissimilar spectral responses might be observed from the same cover type when viewed from an instrument with a wide field of view or between lines where the flight direction has changed.

Studies have shown that most surfaces reflect solar radiation anisotropically (Kreibel 1978, Norman et al. 1985, Kimes et al. 1986, Deering et al. 1992). Vegetated surfaces complicate the effects of bidirectional reflectance because of associated biophysical variables including plant structure, density, leaf area index, and leaf geometry (Walthall 1997). Other factors affecting bidirectional reflectance are atmospheric conditions, topography, scene background characteristics, and wavelength (Pons and Sole-Sugraines 1994, Walthall 1997). The result of bidirectional reflectance is brightness variations within a scene that change spatially and with cover type, and that affect spectral information extraction (Kennedy et al. 1997).

Because of the impact of bidirectional reflectance on quantitative analysis of remotely sensed data, many studies have focused on modeling the geometric parameters of sun and sensor view angles (Royer et al. 1985, Irons et al. 1986, Walthall 1997). Several studies emphasized that vegetation surface drives bidirectional reflectance due to complex shadowing and scattering effects, but found these parameters were difficult to model (Holben and Kimes 1986, Jackson et al. 1990, Mouginis-Mark et al. 1994, Qi et al. 1994, Schaaf and Strahler 1994). Three-dimensional and ray tracing models have been derived to model multilayered canopy reflectance (Kimes and Kirchner 1982, Myneni et al. 1992, North 1996); such models are computationally intensive, impractical for large datasets (satellite imagery), and beyond the scope of many applied remote sensing objectives (Dymond et al. 2001). Physically based models examine the mechanisms that influence reflectance at the surface of the plant including leaf orientation, shape, and layering, and shadowing and backscattering effects (Sandmeier et al. 1998, Dymond et al. 2001). Physical models can become overly complex and measurement intensive, hindering their use in practical applications (Walthall 1997, Dymond et al. 2001). Other physical models have been simplified by reducing the number of parameters (Dymond et al. 2001).

Empirical corrections, while they do not directly address the physical processes of reflectance at the plant surface, are straightforward, require simple measurements, and have modeled bidirectional reflectance with success (Royer et al. 1985, Walthall et al. 1985, Ranson et al. 1991, Kennedy et al. 1997). Empirical models describe the geometry of the sun, target, and sensor, applying this analytical function to every pixel in the scene. An empirical model tested on hyperspectral imagery preserved between-band spectral shape and provided qualitative visual improvement (Kennedy et al. 1997). Spectral band ratioing and vegetation indices such as the normalized difference vegetation index (NDVI) provide a very simple approach for moderating brightness variations across space that result from view angle effects (Royer et al. 1985, Huete et al. 1992). Band ratios do not preserve the original spectral information. Larger bandwidth ratios do not reduce variation as well as shorter bandwidths (Royer et al. 1985, Cihlar et al. 1994).

Methods for modeling bidirectional reflectance range from measurement intensive and computationally complex derivations to simple band ratioing techniques. While a large number of bidirectional reflectance corrections have been described in the literature, no single function has proven universal. For many remote sensing applications, a balance must be struck between theoretical correction and operability.

Influence of Spatial and Spectral Resolution on Classification

Two important factors of remote sensing that impact feature discrimination are the spatial and spectral resolution of the sensor. Spectral classification approaches that enhance vegetation structural, morphological, and phenological characteristics such as canopy height, leaf area and geometry, surface construction, water content, pigmentation, flowering period or senescence, and interaction with shading and background reflectances will have the most success at species differentiation (Knipling 1970, Woolley 1971).

Spatial Resolution

In remote sensing, spatial resolution is the minimum unit on the ground that is represented by the resolution cell size of the imagery, and it is considered synonymous with scale (Woodcock and Strahler 1987). At the beginning of NASA's Earth Resources Technology Satellites (ERTS) program in the 1970s, spatial resolution was limited to relatively coarse-resolution sensors such as the Landsat Multispectral Scanner (MSS) (80 m) (Lillesand and Kiefer 2000). Later, the Advanced Very High Resolution Radiometer (AVHRR) (1.1 km) was launched by the National Oceanic and Atmospheric Administration (Lillesand and Kiefer 2000). Moderate spatial resolution sensors became available to the remote sensing community with the next generation of satellites such as Landsat Thematic Mapper (TM) (30 m) and the French Systeme Pour l'Observation de la Terre (SPOT) satellite (20 m). With the advent of moderate resolution satellites, it was assumed higher spatial resolution would enhance the ability to correctly classify land cover (Irons et al. 1985). Studies comparing the coarse spatial resolution of MSS imagery to the moderate resolution of TM imagery found varying results (Townshend 1980). While greater spectral resolution and radiometric resolution increased classification accuracy, the effect of increased spatial resolution often counteracted the improvements and resulted in lower classification accuracies (Williams et al. 1984, Irons et al. 1985).

The effect of increased spatial resolution on classification is driven by the spatial structure of a scene, or the interaction of spatial resolution and scene complexity (Woodcock and Strahler 1987). Increasing the ground resolving power increases the variability of surface components captured within pixels (Townshend and Justice 1981). For example, the 80 m cell size of an urban area covers a diversity of scene components including interspersed man-made and green-space features. These features are integrated into one spectral response. Conversely, 30 m pixels representing this same area reflect more variability between scene components. A pixel-based classifier such as a maximum likelihood algorithm would accommodate such variability with uncertainty in assigning class membership and reduced classification accuracies (Irons et al. 1985, Lillesand and Kiefer 2000). Local variance is a function of the spatial resolution used to examine the particular environment and the information extracted is dependent on this interaction between resolution and spatial frequency of the environment (Woodcock and Strahler 1987).

Another effect of increased spatial resolution is a reduced number of mixed pixels (Pitts and Badhwar 1980). Mixed pixels result when the resolution cell size is larger than the spectrally unique components of the landscape, and thus the spectral radiance from several components are integrated into one mixed signal. For pixel-based classifiers, there is no retrieval of individual components at the sub-pixel level. Pure pixels are less ambiguous than mixed or boundary pixels and therefore are more accurately classified (Irons et al. 1985). When only classifying pure pixels, one study found that accuracy decreased significantly from 80 m to 30 m resolution due to enhanced within-class variability (Irons et al. 1985). When analyzing pure and mixed pixel data, the decrease in mixed pixels because of the increased resolution counteracted the detrimental effect of pixel variability and there was no change in accuracies from 80 to 30 m (Irons et al. 1985). Ultimately, the effect of increased spatial resolution depends on the spatial structure of the landscape, the complexity of the classification scheme, and the objectives of the classification (Irons et al. 1985, Woodcock and Strahler 1987). High spatial resolution might not be necessary or preferable in order to map coarse land cover classes such as urban, forest, agriculture, and water. On the other hand, greater resolving power might enhance fine spatial scale information content.

Spectral Resolution

Spectral resolution refers to the number and relative width of bands in which reflected electromagnetic energy is measured. While remote imaging systems capture the landscape in a spatial X and Y dimension for each pixel, they also measure multiple Z dimensions consisting of slices of spectral bands that sample reflected and emitted light from an object in the visible through the thermal infrared portions of the spectrum. In effect, each wavelength of energy reflected or emitted is a possible dimension. Multispectral sensors such as Landsat TM are designed to sample discrete portions of the spectrum that have proven, applied value for features such as vegetation, soil moisture, or minerals, and several detectors sample reflected light in relatively coarse bandwidths (Lillesand and Kiefer 2000). Hyperspectral sensors sample reflected energy in many very narrow, contiguous bands and have much greater spectral dimensionality. Such dimensionality becomes important when comparing absorption features or when comparing features statistically. Earth surface features exhibit distinct reflectance patterns, but similar species, minerals, or soils are not always unique or separable (Price

1994), as is often the case with vegetation. The subtleties of high resolution spectral behavior can be underrepresented or lost in broad bands (Lillesand and Kiefer 2000).

There is ongoing discussion within the remote sensing community that hyperspectral data results in more spectral information than necessary (Boardman and Green 2000), and because of the strong correlation between bands, the true dimensionality of the data is much less than the total number of spectral bands. Price (1997) found that of the 224 spectral channels of the Advanced Visible Infrared Imaging Spectrometer (AVIRIS), 30-40 provided maximum information content of reflectance spectra. In practical applications, the true spectral and spatial functionality might best be measured by the ability of the sensor to meet the task objective. For example, one study compared AVIRIS hyperspectral imagery to SPOT multispectral imagery, both with a spatial resolution of 20 m (Ustin and Xiao 2001). Maps of boreal forest successional types revealed that the AVIRIS classification was nearly twice as accurate as the SPOT classification (Ustin and Xiao 2001). Another study of forests in Oregon found that multitemporal Landsat TM data outperformed AVIRIS and high spatial resolution imagery for identifying certain structural variables (Lefsky et al. 2001). The mapping objective and the targeted variables should drive the choice of remote sensing product (Lefsky et al. 2001). Continued research into the effects of high spatial and spectral resolution imagery for assisting with vegetation studies will promote understanding of the relationships between spatial and spectral resolution and ability to predict variables of interest.

Classification Algorithms

Image analysis and classification techniques are expanding as the interest in applying remote sensing imagery to investigate ecological relationships increases (Lees and Ritman 1991, Treitz et al. 1992, Hansen et al. 1996, Lewis 1998, Lawrence and Wright 2001). Traditional multispectral classification techniques, such as the Gaussian maximum likelihood classifier, do not perform as efficiently on hyperspectral imagery (Lillesand and Kiefer 2000). We used two algorithms to classify Probe-1 hyperspectral imagery: Spectral Angle Mapper (SAM) and classification and regression tree (CART) analysis.

In a mapping study for *E. esula*, AVIRIS imagery transformed with simple vegetation indices and NDVI were compared to classifications by SAM and linear spectral unmixing (O'Neill et al. 2000). SAM applied to a minimum noise fraction transformed image (a transformation similar to principle components analysis and incorporated in commercial image processing software) produced the best results (O'Neill et al. 2000).

CART analysis has also shown promise with classifying multispectral and hyperspectral imagery (Hansen et al. 1996, Lawrence and Wright 2001, Lawrence and Labus In press). CART is useful with hyperspectral imagery because it can be used with non-normally distributed data (Hansen et al. 1996). CART identifies the explanatory variables that best explain the response variable thus reducing data dimensionality, and it exposes relationships between the explanatory and response variables (Hansen et al. 1996). CART can also be applied to different data types and does not require expert knowledge (Lawrence and Wright 2001). CART performed better than a maximum likelihood classifier in separating woody from non-woody vegetation in global AVHRR imagery (Hansen et al. 1996). A comparison of CART and discriminant analysis for classifying stress stages of *Pseudotsuga menziesii* (Mirb.) (Douglas-fir) found that CART resulted in substantially higher accuracies (Lawrence and Labus In press). CART was able to select the bands that maximized spectral separability between healthy and stressed trees (Lawrence and Labus In press).

Mapping Plant Species with Remote Sensing

Expanding technologies of airborne and satellite imaging systems and computing capabilities have resulted in increasingly diverse methods for mapping plant species (Anderson et al. 1993, Phinn et al. 1999, Cochrane 2000, O'Neill et al. 2000). The Remote Sensing Unit of the United States Department of Agriculture's Agricultural Research Service (ARS) has devoted considerable time and effort to mapping invasive rangeland species using aerial photography, videography, and satellite imagery (Everitt and Escobar 1996). Aerial photography has a very high spatial resolution, but the spectral resolution is limited because of the lower dynamic range of film emulsion (Lillesand and Kiefer 2000). Regardless of the low spectral sensitivity, the ARS has found aerial photography particularly suitable for mapping a wide variety of undesirable rangeland plants because of the high spatial and textural resolution (Everitt et al. 1995b, Everitt and Escobar 1996).

Videography has gained interest for mapping plant species because of its easy output into digital format and computerized classification, increased radiometric sensitivity to light than that of film, real-time data capture and analysis, and reduced cost (Everitt and Escobar 1992, Neale 1997). Conversely, video images have lower spatial resolution than air photos and cover less area per scene (Neale 1997). The ARS used videography to identify *Opuntia lindheimeri* Engelm. (pricklypear cactus) (Everitt et al. 1991), to map the regional distribution of the two woody species *Acacia rigidula* Benth. (blackbrush acacia) and *Acacia farnesiana* (L.) Willd. (huisache) in south Texas (Everitt et al. 1993b), to detect and map *Astragalus mollissimus* var. *earlei* (Rydb.) (Big Bend loco) and *Astragalus wootonii* Sheld. (Wooton loco) (Everitt et al. 1994), and to distinguish *Euphorbia esula* L. (leafy spurge) from other species (Everitt et al. 1995a). Multispectral videography has been used to classify wetland vegetation and calculate floodplain extent (Neale 1997). Part of a larger riparian restoration project, the vegetation maps were used to identify restoration zones and were valuable as a benchmark resource to monitor the ecological and geomorphic effects of management and restoration. None of the preceding literature, however, provided any form of accuracy assessment that compared airborne video imagery to ground reference. Without some form of accuracy assessment, the quality of a map and fitness for a particular application is uncertain (Janssen and van der Wel 1994, Stehman 1997).

Multispectral satellite imagery has been used to map general land cover extensively, however, the utility of satellite spectral data alone for identifying and mapping specific plants is arguable (Lees and Ritman 1991) because of the relatively coarse spatial resolution of the sensors and the variability of vegetative spectral responses (Price 1994, Cochrane 2000). Landsat TM imagery has been used to predict environmental types at risk of being invaded by *Isatis tinctoria* L. (Dyers woad) by identifying habitat where the invasive plant had prevalently invaded (Dewey et al. 1991). The moderate spatial resolution of Landsat imagery was more suited to identifying associated habitat types than locating singular species. In New Mexico, researchers used supervised classification to identify moderate and light infestations of *Gutierrezia sarothrae* (Pursh) Britt. & Rusby. (broom snakeweed) over large areas using multitemporal AVHRR imagery (Peters et al. 1992). Ground-truthing to assess the accuracy of the map was not performed. SPOT imagery, with a 20 m pixel size, was used to map infestations of two undesirable shrubs in Texas rangelands (Anderson et al. 1993, Everitt et al. 1993a).

Airborne digital imaging systems provide another option for remote vegetation studies, and these platforms provide higher spatial resolution than satellite imagery. The Airborne Data Acquisition and Registration (ADAR) 5500 system is a high spatial resolution multispectral sensor developed initially by NASA, now commercially available, that researchers have used for measuring and monitoring vegetation (Carson et al. 1995, Lass et al. 1996, Phinn et al. 1999, Coulter et al. 2000). A plant community-level mapping project in California compared a map generated by automated classification of ADAR imagery to a map produced by intensive ground mapping methods (Coulter et al. 2000). Although the overall accuracy of the ADAR classified map was about 10% less than the ground-based map, researchers felt the time and effort saved by automated mapping was justified. The classified map identified the more prevalent chaparral community with much greater accuracy than the sensitive coastal sage scrub habitat (Coulter et al. 2000).

In Idaho, invasive plant ecologists have been experimenting with remote sensing to detect and map invasive plants (Carson et al. 1995, Lass et al. 1996, Lass and Callihan

1997). In several studies utilizing ADAR imagery, researchers discovered that weed cover, phenology, and spatial resolution impacted the accuracy of the classification (Carson et al. 1995, Lass et al. 1996, Lass and Callihan 1997). A study of *Hieracium pratense* Tausch (yellow hawkweed) revealed that trying to detect patches with less than 95% cover resulted in confusion with other percent cover classes and the non-weed class (Carson et al. 1995). When lumping three discrete cover classes into a single class, user's accuracy for *H. pratense* jumped to 95% while producer's accuracy increased to 81%. A similar study of *H. pratense* and *Chrysanthemum leucanthemum* L. (oxeye daisy) found that timing image capture to coincide with peak flowering consistently improved the classification accuracy (Lass and Callihan 1997). In a third study comparing four different spatial resolutions ranging from 0.5 m to 4 m, overall accuracy decreased as spatial resolution increased (Lass et al. 1996), indicating that there might have been an optimal resolution for use in that particular environment where local variance was minimized and the ratio of pure pixels to boundary pixels maximized, thus improving classification.

Sensors with high spectral resolution (hyperspectral) and variable spatial resolution have also been utilized in vegetation studies. Hyperspectral imagery has been used to map oak savanna-grassland in California (Ustin et al. 1996), a mosaic of chaparral community types (Roberts et al. 1998), boreal forest cover types in Canada (Fuentes et al. 2000) and Alaska (Ustin and Xiao 2001), and composition of an eastern mixed deciduous forest (Martin et al. 1998). These applications identified relatively broad cover classes or green vegetation in general, and have not been used to target specific plants.

In addition, the use of spectral mixture analysis (SMA) with hyperspectral imagery has allowed fractions of constituent components in a 20 m AVIRIS pixel to be quantified. In effect, the SMA process reduces the limitations imposed by coarser spatial resolution and mixed pixels, however it assumes that linear mixing occurs between components (Adams et al. 1993, Roberts et al. 1993, Roberts et al. 1998), which is not always the case when leaf canopies induce multiple scattering of light (Roberts et al. 1998). Uncertainty has been encountered using SMA in arid and semi-arid environments, because the background constituents, predominantly soil, overwhelm the weak vegetation signal (Okin et al. 2001). Okin et al. (2001) warned that even hyperspectral technology is limited by the physical environment and type of vegetation, and they estimated that indeterminate vegetation spectra typical of arid regions makes retrieval of species information unreliable below 50% cover. Further, even vegetation that exhibits some spectrally unique attributes is difficult to unmix at covers below 10% (Okin et al. 2001). The ultimate challenge with identifying plant species remotely based on reflected light is that the spectral response of vegetation is both highly variable and non-unique (Price 1994, Cochrane 2000).

While the process of remote sensing to the species level has not been perfected to date, it nevertheless offers tradeoffs between traditional mapping methods, such as time and cost savings, which make it a potentially valuable tool. Recently AVIRIS imagery was used to map woody plant encroachment into grasslands (Wylie et al. 2000) and to update maps of the noxious plant *E. esula* in a national park (O'Neill et al. 2000). With continued research and application to resource issues, land managers and ecologists will be able to make informed decisions about which remote sensing products might best meet management objectives.

Data Reliability: Thematic Accuracy Assessment

To provide users of remote sensing data with information about map reliability or fitness for use, it is important that an accuracy assessment be performed to compare the classification or predicted data to reference data or ground truth. In the early days of remote sensing, classified maps would be visually compared to a known reference map or area and pronounced adequate with little or no quantitative summary of accuracy. (Congalton 1991). Scientifically objective methods based on probability sampling and multivariate analysis have evolved that allow statistical estimation and inference (Congalton et al. 1983, Congalton 1991, Stehman 1997). Satisfying the appropriate assumptions and requirements of statistical theory remains challenging when time and cost is often a limiting factor in applied research and management (Stehman 2001).

A fundamental component of an objective accuracy assessment is the sampling design (Congalton and Green 1999). The sampling design is the methodology used to select the units of reference that are used in both the training portion of classification and the analysis or comparison. The sampling design estimates the true population, or the entire area mapped and must be representative of that population for inference to be extended beyond the sample. Design-based estimation must also be based on probability sampling to make inference about the population (Stehman and Czaplewski 1998). Stehman (2001) argues that independence and equal probability are not required of the descriptive analysis common to most accuracy assessments, rather, descriptive inference is satisfied if the probability of including all elements in a sample is known. If the probability of including a sample element is known to be zero, then inference beyond that sample element is invalid. Common sampling schemes such as simple random, stratified random, systematic, and clustering adhere to the probability sampling requirement (Congalton 1991, Stehman and Czaplewski 1998, Stehman 2001). Subjective sampling based on convenience or accessibility does not allow inclusion probabilities to be determined and is not reliably representative (Stehman and Czaplewski 1998).

The sampling unit provides the basis for confirming a match between a class on the map and the corresponding class on the ground or reference map. The link provided by the sampling unit is both thematic and spatial. Sampling units can be points or area units such as pixels, polygons, or pixel clusters (Stehman and Czaplewski 1998). Janssen and van der Wel (1994) recommend the pixel because raster imagery is composed of pixels and is therefore most appropriate if pixel-based classification is performed. Pixels are difficult to locate accurately (Aronoff 1985), therefore, blocks of pixels are often used instead. The choice of sampling unit is often guided by mapping objective, management purpose, features of the physical environment, and feasibility (Stehman and Czaplewski 1998, Congalton and Green 1999). If the user requires information about invasive plant infestations, then the polygon is more ecologically representative of the management need.

Image classified and field reference sample data are compared in an error matrix, or contingency table, and several estimation parameters computed to describe accuracy. There is no agreement on a single summary measure of accuracy or even which measure might best represent a particular objective (Stehman 1997), yet the Kappa statistic is often cited, relatively easy to compute, and recommended by several researchers (Congalton et al. 1983, Rosenfield and Fitzpatrick-Lins 1986, Hudson and Ramm 1987, Foody 1992, Janssen and van der Wel 1994, Congalton and Green 1999). Kappa was first introduced in the psychology literature by Cohen (1960) as a method to compensate for chance agreement between two comparisons in a contingency table. Congalton and Green (1999) cited the first publication of the Kappa statistic as a tool for remote sensing investigations as Congalton et al. (1983). Since then, Kappa and conditional Kappa, which mitigates chance agreement within individual classes, have been recommended for effectively representing overall and class accuracies (Rosenfield and Fitzpatrick-Lins 1986, Fitzgerald and Lees 1994). Kappa has been shown to overestimate random agreement and underestimate accuracy, therefore a modified Kappa was proposed (Foody 1992). Ma and Redmond (1995) recommended Tau, a derivation of Kappa, based on *a priori* rather than *a posteriori* probabilities of group membership. While agreement about the propriety of using Kappa as an overall measure of accuracy is disconsonant, Kappa does afford a method for comparing different classifications and remains a useful statistic for remote sensing (Congalton and Green 1999).

Ultimately, the accuracy measures used to represent a classification should reflect the objectives of the mapping project. If the sampling strategy follows statistically rigorous protocols, then the overall, user's, and producer's accuracies are valid estimates of the population error matrix (Stehman 1997). The entire error matrix should be presented with summary measures of the overall accuracy for all categories and user's and producer's accuracy for each category (Stehman 1997). If summary measures of the error matrix are presented, users are provided with information about where confusion exists between classes and what classes are being omitted. This allows the user to consider the costs of misclassification or omission. In terms of invasive plant mapping, there might be greater economic cost involved in false positives; visiting a field location that the map indicated was infested by the plant only to find no infestation would result in time wasted. In such a case, user's accuracy for the invasive plant category is the important accuracy parameter. From an ecologic standpoint, however, there might be greater cost associated with omitting the invasive plant, and thus never targeting the location for management. Missing an infestation and allowing the species to spread might be ecologically costly. By presenting overall, user's, and producer's accuracies, multiple parameters of interest are disclosed, and ultimately accuracy information is available to multiple users with potentially different objectives. If sound statistical sampling methods are used, the user can draw inferences about the population represented by the map (Stehman 1997).

Summary

Remote sensing products have been widely utilized in vegetation studies (Wessman et al. 1997, Price et al. 2001). Satellite imagery has been extensively used to map generalized land cover and vegetation biomass since the launch of NASA's Landsat series (Graetz and Gentle 1982, Sohn and McCoy 1997). Air photo interpretation has been used to map plant species that exhibit unique visible pigment or morphological characteristics (Ramsey et al. 2002). Airborne digital imagery can provide greater spectral sensitivity than air photos, with comparable spatial resolution (Lillesand and Kiefer 2000). Commercial sensors have been developed that offer both high spatial resolution and spectral resolution. Tradeoffs between spatial and spectral resolution for taxonomic mapping have been debated (Price 1997, Boardman and Green 2000). Imagery with high spatial and spectral resolution, however, might provide the spatial detail and the sensitivity to minor spectral deviations necessary to differentiate between plant species.

CHAPTER 3

DETECTING AND MAPPING LEAFY SPURGE AND SPOTTED KNAPWEED IN RANGELAND ECOSYSTEMS USING AIRBORNE DIGITAL IMAGERY

Introduction

Invasive nonindigenous plants are harmful ecologically and economically to North American rangelands (Sheley et al. 1996, Vitousek et al. 1996, Bangsund et al. 1999). Effective and dynamic invasive plant management plans are critical for preventing and minimizing the spread of undesirable species (Sheley et al. 1999b). Invasive plant management plans require accurate and timely spatial information concerning the distribution of both undesirable plant species as well as desirable vegetation communities (Sheley et al. 1996). Accurate infestation information assists with locating and controlling small infestations before they grow too large to eradicate effectively (Johnson 1999). Timely and repeated mapping allows managers to monitor change in weed distributions and thus the effectiveness of their management strategies (Cooksey and Sheley 1997).

Traditional survey methods for noxious weeds have utilized ground-based methods such as hand mapping onto 7.5' topographic quadrangles or directly mapping weed infestations with GPS receivers (Cooksey and Sheley 1997). While these methods specify sufficiently high accuracies (approximately 80%) for small management areas (Cooksey and Sheley 1998a), the intensive, systematic survey methods required to accurately map large areas might be financially, technically, and logistically impractical for many managers. Methods that promote accurate, landscape-scale mapping of rangelands at reduced cost would improve the ability of land managers to detect and monitor invasive plant distributions. For this study, the use of "landscape scale" refers to large geographical areas that have a common land management goal, such as county weed management areas, or state/federal wildlife reserves, grazing allotments, and wild and scenic river corridors.

Remote sensing has been used for decades to measure and map the biophysical characteristics of vegetation (Anderson et al. 1976, Tucker et al. 1985, Ioka and Koda 1986, Smith et al. 1990, Treitz et al. 1992, Phinn et al. 1996, Ustin et al. 1996, Neale 1997, Lawrence and Ripple 2000). Recently, studies have targeted ecologically and economically harmful plants and attempted to devise methods for mapping larger geographic extents (Everitt et al. 1987, Everitt and Deloach 1990, Everitt et al. 1992, Peters et al. 1992, Anderson et al. 1993, Carson et al. 1995, Everitt et al. 1995b, Anderson et al. 1996, Lass et al. 1996, Ramsey et al. 2002). Managers need an alternative mapping methodology when traditional ground-based methods are logistically unfeasible due to large management areas. Remote sensing has the potential to map large areas at more feasible costs.

Detecting Invasive Plants: Spatial and Spectral Resolution

The utility of remote sensing for detecting weed infestations lies in the potential to map accurately large areas using automated techniques that process and classify imagery with relative technological ease. The areal extent that can be mapped by remote sensing depends on the spatial resolution and field of view of the sensor. Moderate spatial and spectral resolution satellite sensors such as Landsat Enhanced Thematic Mapper Plus (ETM+) or Systeme Pour l'Observation de la Terre (SPOT) offer broad area coverage in a single scene, yet at 20-30 m pixel size, the spatial resolution is too coarse generally to distinguish individual species unless represented homogenously (Dewey et al. 1991, Everitt and Escobar 1996, Sohn and McCoy 1997). Further, there is some dispute as to the potential for using remote sensing alone as a tool to discriminate between plant species becuase of the inherent variability in reflectance within species (Lees and Ritman 1991). The utility of remote sensing, however, is perhaps most practically tested by an accuracy assessment.

In contrast to satellite imagery, aerial photography is capable of producing very high spatial resolution (often less than 1 m). The radiometric range of film emulsion is not as wide as the photosensitive devices used in electronic image sensors, nor are the dye layers discrete in the visible portion of the spectrum (Lillesand and Kiefer 2000). In addition, processing, scanning or digitizing, and interpreting conventional aerial photography can be costly, time consuming, and labor-intensive, requiring a trained photointerpretor or knowledge of the site (Everitt and Escobar 1996). Further, mapping has been limited to species that have unique visible characteristics such as a bright color or pubescence (Everitt and Richerson 1987). Generally, vegetation reflectance is too similar in the visible (VIS) and near-infrared (NIR) wavelengths (Woolley 1971, Cochrane 2000, Okin et al. 2001) to delineate spectrally using the limited spectral dynamic range of aerial photography (Lillesand and Kiefer 2000).

Difficulties notwithstanding, aerial photography has been used to map undesirable herbs and shrubs in Texas and New Mexico rangelands (Everitt et al. 1987, Everitt et al. 1992, Everitt et al. 1994) and the riparian invasive shrub *Tamarix chinensis* Lour. (Chinese tamarisk) in Texas and Arizona (Everitt and Deloach 1990). In Montana and North Dakota, *Euphorbia esula* L. (leafy spurge) exhibited significantly higher reflectance in the VIS (red) portion of the spectrum (630 – 690 nm) than associated vegetation (Everitt et al. 1995a). Another species with bright yellow flowering characteristics, *Gutierrezia sarothrae* (Pursh) Britt. & Rusby., was similarly observed to have higher reflectance at the 550 – 650 nm wavelengths (Everitt et al. 1987). Further, *E. esula* differed from most associated rangeland species except *Symphoricarpus albus* (L.) Blake (snowberry), *Melilotus officinalis* (L.) Lam. (yellow sweet-clover), and *Descurainia pinnata* (Walt.) Britt. (pinnate tansymustard), with higher reflectance in the NIR portion of the spectrum (760 – 900 nm). As a result, researchers were able to utilize both VIS and NIR spectral characteristics to photointerpret and map landscape scale infestations of *E. esula* with conventional color and color infrared (CIR) aerial photography in Theodore Roosevelt National Park (Anderson et al. 1996). Many studies, however, do not provide a quantitative accuracy assessment. To make remote weed mapping more feasible, high spatial resolution, high spectral resolution, and automated methods for identifying weed species are needed.

An alternative to both satellite imagery and aerial photography exists in airborne digital imagery. The spatial resolution of such sensors is similar to that of aerial photography, yet methods for processing and spectrally classifying the imagery can be automated, allowing for more efficient landscape-scale coverage. In Idaho, 4-band multispectral imagery captured from fixed wing aircraft and with very high spatial resolution has been used to map several invasive plants (Carson et al. 1995, Lass et al. 1996, Lass and Callihan 1997).

Another variable to consider for detailed invasive species mapping using airborne digital imagery is the spectral resolution of the sensor. Both satellite and airborne multispectral imagery generally utilize relatively wide, discontinuous bandwidths in the visible, near-infrared, middle infrared, and thermal infrared portions of the spectrum. Recent technological advances have combined the principles of spectroscopy with the spatial component of remote imaging to produce hyperspectral sensors that sample electromagnetic energy in very narrow, continuous channels. The result is spectral response curves with very detailed absorption and reflection characteristics, which can facilitate identification of specific materials (Adams et al. 1993).

Because healthy vegetation exhibits similar spectral response in the VIS and NIR portions of the spectrum due to similar cellular chemistry and architecture (Woolley 1971), identifying invasive species in a heterogeneous landscape is difficult with moderate resolution multispectral imagery (Dewey et al. 1991). Because of the continuous nature of spectra inherent to hyperspectral imagery, greater information content of the data might be utilized to differentiate vegetation into taxonomic levels. Researchers have applied hyperspectral imagery for mapping the non-indigenous *E. esula* in Theodore Roosevelt National Park (O'Neill et al. 2000) and to monitor undesirable woody vegetation encroaching into grasslands in the Niobrara Valley (Wylie et al. 2000).

It has been argued that hyperspectral information is redundant and that spatial resolution ultimately provides greater discriminatory power (Price 1997, Boardman and

Green 2000). While independent studies have mapped invasive species with hyperspectral imagery (O'Neill et al. 2000, Wylie et al. 2000) and high spatial resolution multispectral imagery (Carson et al. 1995, Lass et al. 1996, Lass and Callihan 1997), a direct comparison of methodology and results has not yet been published. The purpose of this study was to map *E. esula* and *Centaurea maculosa* Lam. (spotted knapweed) using hyperspectral imagery and high spatial resolution multispectral imagery and to compare the resulting map accuracies. Hyperspectral and multispectral imagery were of different spatial resolutions and were classified with different algorithms. We compared the systems as a whole for their practical utility in mapping the target weeds. The components of the systems included the sensor, spectral resolution, spatial resolution, and classification algorithm.

Methods

Study Sites

The imagery covered two sites in Madison County, Montana, each site approximately 1,024 ha in area (Figure 1). The *E. esula* site was located 16 km southwest of Twin Bridges at the southern end of the Highland Mountains (UTM extents: 384,023E, 5,092,295N and 387,239E, 5,039,036N; NAD83, Zone 12). Average annual precipitation was 30 cm (Boast and Shelito 1989). Physiography predominantly consisted of upland fans dissected with ephemeral streams and terraces of the Big Hole River. Native vegetation was a mix of grasses, forbs, and shrubs, including *Bouteloua gracilis* (H.B.K.)

Lag. (blue grama), *Poa sandbergii* Vasey (Sandberg bluegrass), *Agropyron smithii* Rydb. (western wheatgrass), *Pseudoroegneria spicatum* Pursh. (Love) (bluebunch wheatgrass), *Stipa comata* Trin. & Rupr. (needleandthread), *Stipa viridula* Trin. (green needlegrass), *Artemisia tridentata* Nutt. (big sagebrush), and *Chrysothamnus nauseosus* (Pall.) Britt. (rabbitbrush) (Boast and Shelito 1989). *E. esula* primarily occupied drainage bottoms and surrounding hillsides and was distributed with native vegetation in low to high density infestations.

E. esula is a rhizomatous perennial forb that thrives in a wide range of environmental conditions (Lajeunesse et al. 1999). *E. esula* is aggressive, spreading vegetatively and by exploding seed capsules to grow in dense patches, and is persistent due to nutrient reserves held in deep root systems (Lajeunesse et al. 1999). In full bloom, the leafy bracts of *E. esula* are a bright, showy yellow-green. Senescence occurs after seed production around the middle of August, whereupon the stems, leaves, and bracts dry to a rusty red color. *E. esula* was growing in a variety of phenological stages on the date the image was captured, ranging from bright yellow-green flowering to early senescence. *E. esula* was generally found in low to moderate density patches with other vegetation but occasionally grew in dense monocultures.

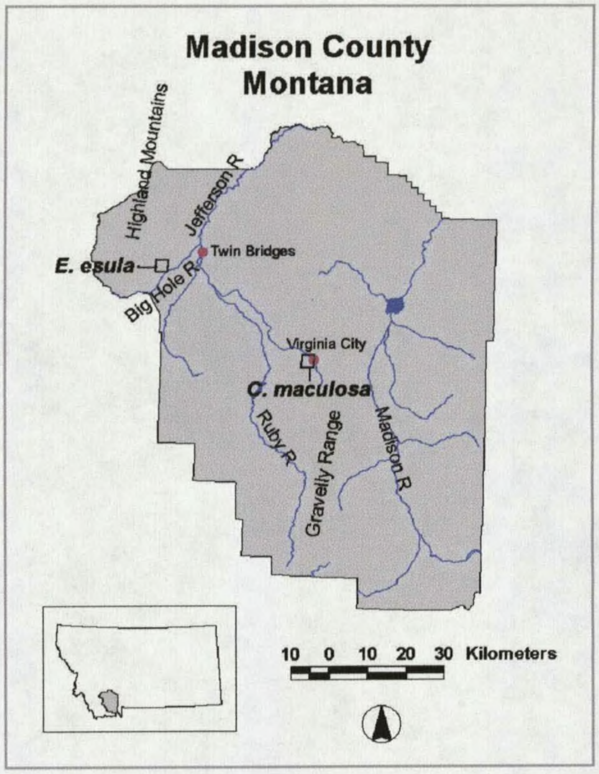

Figure 1. *Euphorbia esula* and *Centaurea maculosa* were mapped at two locations in Madison County, southwest Montana.

The *C. maculosa* site was located in the northern foothills of the Gravelly Range and included the town of Virginia City and areas due west and south (UTM extents: 422,693E, 5,017,404N and 425,887E, 5,014,094N; NAD83, Zone 12). Average annual precipitation was 30 cm (Boast and Shelito 1989). Physiography predominantly consisted of upland hills and ridges of the Gravelly Mountains and floodplains of perennial streams. Native vegetation consisted of mixed rangeland-forest types, including *P. spicatum*, *Festuca idahoensis* Elmer (Idaho fescue), *S. comata*, *Carex filifolia* Nutt. (threadleaf sedge), *Lupinus* L. spp. (lupine), *A. tridentata*, *C. nauseosus*, *Gutierrezia sarothrae* (Pursh) Britt. & Rusby. (broom snakeweed), *Symphoricarpus albus* (L.) Blake (snowberry), *Juniperus scopulorum* Sarg. (juniper), *Populus tremuloides* Michx. (aspen), and *Populus deltoides* Marsh. (cottonwood) (Boast and Shelito 1989). In addition, the non-native grass *Bromus tectorum* L. (cheatgrass) infested portions of the site.

C. maculosa is a tap-rooted, perennial forb that has invaded over 7,000,000 ha in North America since its introduction from Eurasia in the late 1800s (Sheley et al. 1998). Competitive physiology allows *C. maculosa* to displace native species across a wide range of environments (Sheley et al. 1993). Once *C. maculosa* is established, little else grows under its canopy with increased exposure of bare soil resulting (Tyser and Key 1988). *C. maculosa* produces a branched inflorescence of purple flowers from late-June to late-September. Foliage ranges from fresh green during early growth to dull gray-green in later growth. On the date the imagery was captured *C. maculosa* was growing in various phenological stages, from recent flowering to early senescence. *C. maculosa* infestations tended to be mixed with other vegetation and had a higher percentage of bare soil exposed than the *E. esula* site.

Data Collection

The multispectral imagery was obtained using the Airborne Data Acquisition and Registration (ADAR) 5500 sensor, an electronic imaging instrument comprised of four cameras mounted with 20 mm lenses. The *E. esula* site was flown on 7 August 1999 and the *C. maculosa* site on 10 August 1999; both were flown at approximately 11 am

Mountain Daylight Time (MDT). The average flying height of 2225 m above ground level resulted in a nominal spatial resolution of 1 m. Cameras were individually filtered to record reflectance over the ranges 460 – 550 nm, 520 – 610 nm, 610 – 700 nm, and 780 – 920 nm, centering on blue, green, red, and NIR portions of the spectrum, respectively.

The hyperspectral imagery was obtained using the Probe-1 sensor. The *E. esula* and *C. maculosa* sites were both flown on 25 August 1999 from approximately 12 pm to 2 pm MDT. Specifications for Probe-1 cite a ground resolution cell of 5 m when flying at an average height above ground level of 2500 m (Earth Search Sciences 2002). The Probe-1 sensor records incoming light in 128 bands in a nearly continuous spectral range from 440 – 2507 nm.

In August 1999, crews collected ground reference polygons of the target weed (*E. esula* or *C. maculosa*) and associated vegetation using Trimble GeoExplorer II Global Positioning System (GPS) receivers that have an accuracy of 2-5 m after differential correction (Marshall 1996). We randomly located transects within a grid overlaid on the study site and sampled target weed and associated vegetation polygons. Sizes of weed infestations ranged from 6 to 507 m^2. GPS field data were differentially corrected. Samples were split randomly into two sets: (a) image reference spectra for the classification algorithm and (b) ground reference samples for an accuracy assessment. We did not sample a hay meadow in the southeast portion of the *E. esula* study site, nor within the city limits of Virginia City at the *C. maculosa* site. We subsequently masked these areas from the study area.

Image Processing and Analysis

Multispectral Imagery. The multispectral imagery was delivered to us georeferenced (UTM, NAD83, Z12), color-balanced, and mosaicked by Positive Systems, Inc. A root mean square error (RMSE) was not reported. We visually compared the imagery to a DOQ and found excellent co-registration of features. Therefore, the GPS data was directly overlaid onto the imagery to obtain image statistics and perform accuracy assessments.

We used ERDAS Imagine (v. 8.4) image processing software to spectrally classify the imagery with a maximum likelihood (ML) classifier. The ML algorithm used the reference or "supervised" training data to develop statistical decision rules for assigning pixels to a given category. Half of the ground reference samples were used as image reference spectra. For the *E. esula* site, there were 85 vegetation and 48 *E. esula* training classes. For the *C. maculosa* site, there were 88 vegetation 68 *C. maculosa* training classes. Rules were based on probability density functions developed from mean vectors and covariance matrices, and assumed a Gaussian distribution of the training class statistics (Jensen 1996). Class probabilities of occurrence were weighted equally for all classes. Post-classification smoothing was applied using a 3x3 majority filter to mitigate the inherent speckled nature of the remotely sensed classification.

Hyperspectral Imagery. We used a polynomial transformation to georegister the hyperspectral imagery to a DOQ. The transformation did not adequately correct local distortion and produced high RMSEs (2 – 14 pixels or approximately 10 – 70 m). To compensate for poor co-registration, we interactively moved the GPS reference polygons to correspond with visual locations on the DOQ. We acknowledged a certain degree of locational inaccuracy because of accuracy limitations of the DOQ (USGS 2001) and the difficulty of visually co-registering pixels. We did not attempt to quantify the potential spatial error resulting from relocated polygons.

After georeferencing, we resampled images of the *E. esula* site to 5 m pixels using a nearest neighbor function and mosaicked five scenes into one composite image. Illumination variations within and between scenes were not corrected for the *E. esula* imagery. We observed distinct and potentially problematic illumination differences between scenes at the *C. maculosa* site, so we applied a cross-track illumination correction (CTIC) incorporated into ENVI (v. 3.2) image processing software (ENVI 1997). We measured pixel sizes and observed an average pixel size of approximately 3.5 m. After CTIC we resampled images to 3 m pixels using a nearest neighbor function.

We tested two different classification approaches. We used Spectral Angle Mapper (SAM), an algorithm incorporated into ENVI (ENVI 1997), and a rule-based system using classification and regression tree analysis (CART) (Breiman et al. 1984). To simplify comparison, in this section we present the multispectral ML classification and the hyperspectral CART classification. The hyperspectral SAM classification is presented and compared to the multispectral ML and hyperspectral CART classifications in Appendix A.

CART analysis is a statistical technique that clusters data into homogenous terminal nodes, or classes, on a hierarchical tree using recursive partitioning (Lawrence and Wright 2001). CART iteratively examines and splits all predictor variables into binary nodes that produce best homogeneity, or minimized deviance of the response variable.

Ultimately, a tier of decision rules are generated that utilize those predictor variables that best predict purest class membership.

We generated classification trees in S-Plus 2000 statistical software and pruned the trees according to cross-validation procedures (Venables and Ripley 1997). Cross-validation produced a plot of the amount of deviance in class type reduced at each node of the tree. Trees were pruned where insubstantial reduction of deviance occurred. Pruning simplified a potentially overfit model, eliminating those splits that explained minimal deviance in the dataset (Lawrence and Wright 2001). The result was a series of decision rules using the explanatory power of those spectral bands most efficient at differentiating pixels into target weed or associated vegetation class membership. The decision rules were used in Imagine's Expert Classifier module to create maps. A 3x3 majority filter was applied to the classified image to smooth inherent variability.

Accuracy Assessment

Both multispectral and hyperspectral image classification resulted in hard classification of pixels: each pixel was assigned to only one category. Thematic maps of target weed and associated vegetation were generated from each classified image. Accuracy assessments were performed that compared the predicted cover class (classified map) to observed cover class (GPS reference data). Error matrices were created for each classified image and overall accuracy, producer's accuracy, and user's accuracy were calculated.

Overall accuracy measures complete agreement between map and reference data, however, it provides no information about performance of individual classes or where class confusion might occur (Rosenfield and Fitzpatrick-Lins 1986, Story and Congalton 1986). Producer's accuracy measures the proportion of units correctly classified out of the total number of reference units for each category. A measure of the algorithm's success at identifying classes, it provides information about observations that have been omitted from the correct category. User's accuracy indicates the proportion of units correctly classified into the appropriate category out of the total units classified into each map category. It reveals where errors by commission have occurred, or when a unit has been placed into the wrong category. While we present all summary measures from the error matrices, we focus on user's accuracy. From a management perspective, user's accuracy provides more valuable information about the classification accuracy or effectiveness of the map because it indicates the proportion of target weed units on the map where a map user would actually find the target weed on the ground.

In addition to the error matrix, we performed a Kappa analysis, a discrete multivariate statistical technique used to compare categorical classifications (Cohen 1960, Congalton et al. 1983, Rosenfield and Fitzpatrick-Lins 1986, Hudson and Ramm 1987). The Khat statistic, an estimate of the Kappa coefficient of agreement, was used to measure the difference in agreement between each remotely sensed classification and any agreement resulting from each unique classification because of chance (Congalton and Green 1999). For each classification, chance agreement was calculated from the observed marginal proportions of the error matrix (Stehman 1997), thus each classification was compared to its own unique potential for chance agreement. In this study, we were not comparing algorithms directly because other variables (spatial and spectral resolution, sensor) were not held constant (Table 1). Because of differences in spatial and spectral resolution and sensor, one could not make the claim the algorithm caused the increase in accuracy. As a result, we could not use Kappa to compare different classifications for significant differences.

Table 1. Imaging systems and methods of analysis compared for (a) *E. esula* site and (b) *C. maculosa* site. Sensor, bands, spatial resolution, and classification algorithm are compared.

E. esula		
ADAR 5500 4-band 1 meter ML	compared to	Probe-1 128-band 5 meter CART

(a)

C. maculosa		
ADAR 5500 4-band 1 meter ML	compared to	Probe-1 128-band 3 meter CART

(b)

The sample units used for the accuracy assessment were polygons. Because the strictest interpretation of correctly classified vegetation and weed polygons was unrealistic for the resulting discrete thematic maps (weed infestations were not 100% infested), decision rules for determining whether a given reference polygon overlaid on the raster classification map was correctly classified followed incremental percentage thresholds. For example, in the strictest interpretation, or 0% threshold, no weed pixels should be present in a polygon in order to be correctly classified as vegetation, while one weed pixel in a given polygon would constitute correct classification as the target weed. The classifications inherently resulted in some degree of speckle and a hard interpretation tended to produce unrealistically low accuracies. For example, few vegetation accuracy assessment polygons contained solely vegetation pixels. Accuracy thresholds were calculated in 5% increments that increased for vegetation, or limited for weed, the percentage of non-category pixels allowed for a correct classification. For example, at the first 5% increment, a polygon scored a correct classification as the target weed if it contained at least 5% weed pixels. On the other hand, a polygon scored a correct classification as vegetation if it contained less than 5% weed pixels.

We produced accuracy assessment plots, starting at the strict 0% threshold rule, which graphed user's accuracies for target weed (of most interest to a weed map user) and vegetation classes, overall accuracies, and Khat statistics at 5% threshold intervals. We generated error matrices for the strict 0% threshold rule and for the threshold that optimized user's accuracy for the target weed without a decline in overall accuracy.

Results

Euphorbia esula

Multispectral Imagery. Using the strictest interpretation of accuracy (0% threshold), user's accuracy for *E. esula* was 41%, user's accuracy for vegetation was 83%, overall accuracy was 50%, and the Khat value was 0.14 for the classified map (Table 2). At the 0% threshold there was substantial confusion of vegetation for *E. esula* because of widely distributed speckle that caused most vegetation polygons to contain at least some weed pixels. At the strict interpretation, vegetation polygons were to be weed free. The map visually revealed overclassification of *E. esula*, with widely scattered, low-density infestations across the landscape, and a slight pattern of clustering in drainages (Figure 2). As the thresholds became less stringent, all accuracies increased. At the 10% threshold, the Khat value was maximized at 0.44, while user's accuracy for vegetation peaked at 87%, user's accuracy for *E. esula* was 57%, and overall accuracy was 71% (Figure 3). User's accuracy for *E. esula*, however, continued to rise and at the 50% threshold achieved an accuracy of 84%. Thereafter, overall accuracy declined from the high of 74%. At the 65% threshold no vegetation polygons were misclassified (all vegetation polygons were composed of at least 35% vegetation pixels) therefore user's accuracy for *E. esula* jumped to 100%.

Hyperspectral Imagery. Using the strictest interpretation of accuracy for the CART classified map, user's accuracy for *E. esula* was 61%, user's accuracy for vegetation was

74%, overall accuracy was 70%, and the Khat value was 0.32 (Table 2). The hyperspectral CART map revealed a more concentrated (less diffuse) pattern to the *E. esula* infestations, with distributions clustering in drainages and on hillslopes nearby (Figure 2). As thresholds became less strict, user's accuracy for vegetation showed little change (Figure 3). User's accuracy for *E. esula* climbed steadily as classification rules for vegetation relaxed (we accepted more weed pixels in vegetation polygons) and fewer vegetation polygons were confused with weed polygons. User's accuracy for *E. esula* reached 82% at the 50% threshold. At this point, overall accuracy was maximized at 75% and the Khat value reached a high of 0.38.

Table 2. Error matrix summary measures comparing multispectral classification and hyperspectral classification of *E. esula* at strict interpretation of accuracy (0% threshold) and 50% threshold.

Multispectral Classification Accuracies			**Hyperspectral Classification Accuracies**		
0% Threshold			**0% Threshold**		
%	*E. esula*	Vegetation	%	*E. esula*	Vegetation
User's	41	83	User's	61	74
Producer's	90	28	Producer's	49	82
Overall	50		Overall	70	
Khat	0.14		Khat	0.32	
50% Threshold			**50% Threshold**		
%	*E. esula*	Vegetation	%	*E. esula*	Vegetation
User's	84	72	User's	82	73
Producer's	33	96	Producer's	38	95
Overall	74		Overall	75	
Khat	0.34		Khat	0.38	

Table 3. Error matrix summary measures comparing multispectral classification and hyperspectral classification of *C. maculosa* at strict interpretation of accuracy (0% threshold) and 45% and 25% thresholds.

Multispectral Classification Accuracies			**Hyperspectral Classification Accuracies**		
0% Threshold			**0% Threshold**		
%	*C. maculosa*	Vegetation	%	*C. maculosa*	Vegetation
User's	45	73	User's	74	62
Producer's	94	13	Producer's	41	86
Overall	48		Overall	65	
Khat	0.06		Khat	0.28	
45% Threshold			**25% Threshold**		
%	*C. maculosa*	Vegetation	%	*C. maculosa*	Vegetation
User's	69	83	User's	86	62
Producer's	68	49	Producer's	37	95
Overall	68		Overall	67	
Khat	0.33		Khat	0.32	

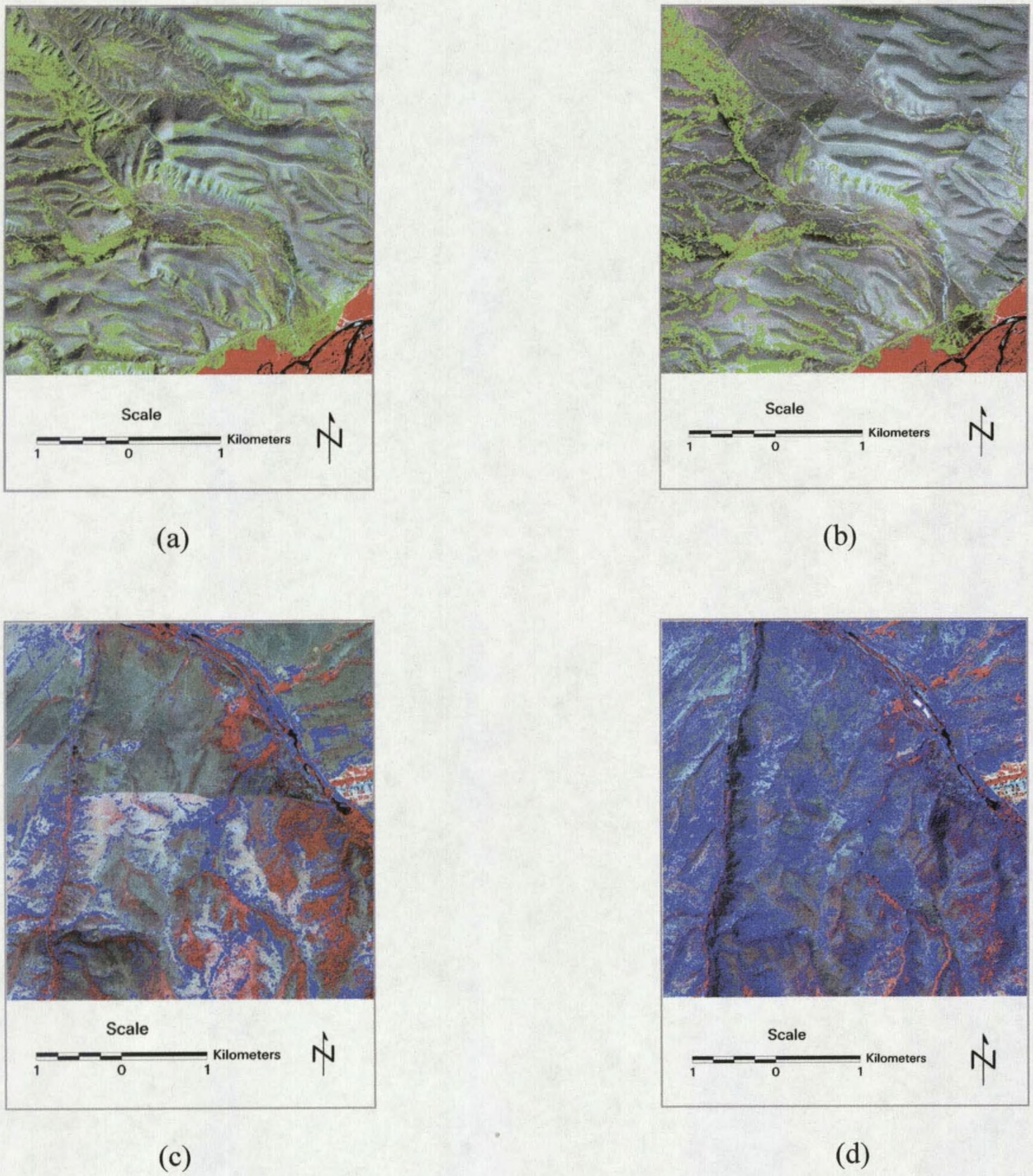

Figure 2. (a) ML classification of *E. esula*, displayed in bright green, overlaid on 4-band multispectral imagery. Bands 4 (780-920 nm), 3 (610-700 nm), and 2 (520-610 nm) are displayed as red, green, and blue. (b) CART classification of *E. esula* overlaid on hyperspectral imagery. Bands 24 (784 nm), 16 (662 nm), and 9 (555 nm) are displayed as red, green, and blue. (c) ML classification of *C. maculosa*, displayed in blue, overlaid on 4-band multispectral imagery. (d) CART classification of *C. maculosa* overlaid on hyperspectral imagery.

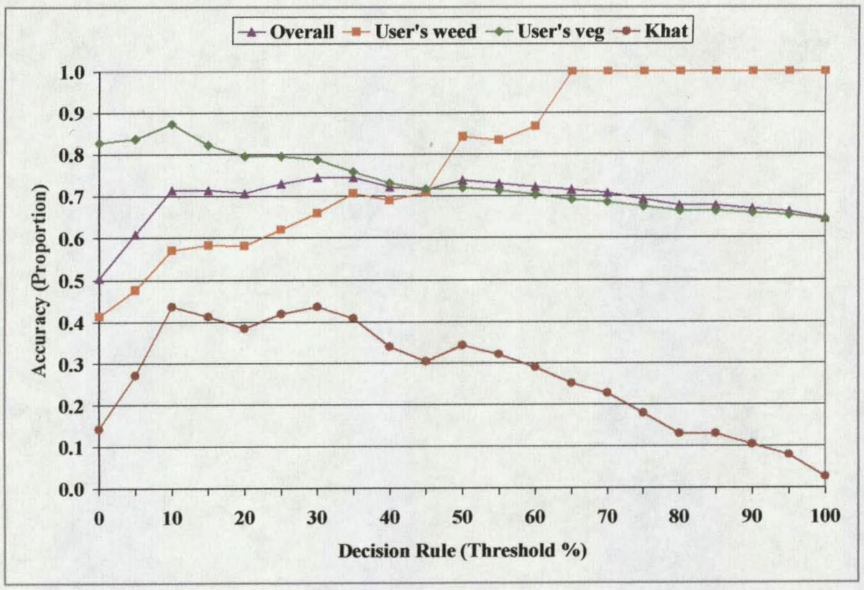

(a)

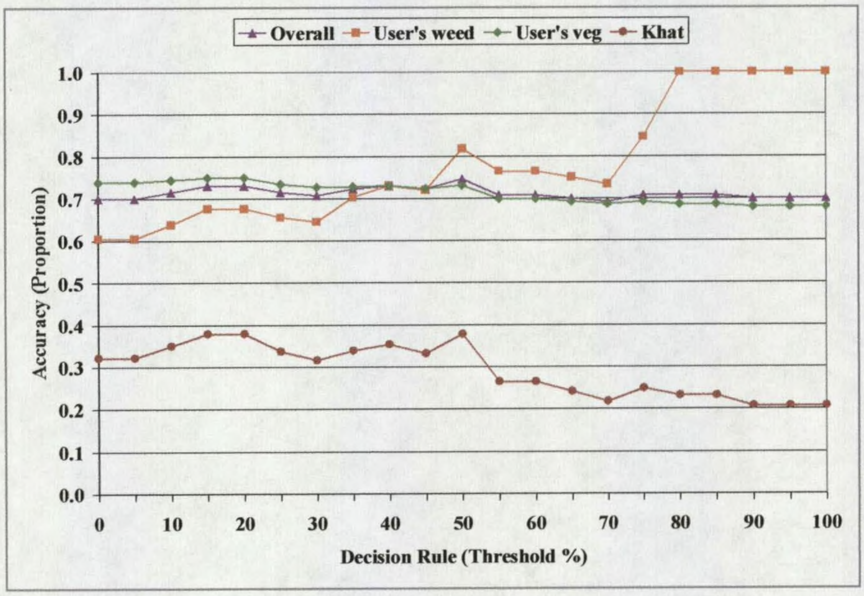

(b)

Figure 3. Accuracy assessment curves comparing incremental decision rules for (a) multispectral ML classification and (b) hyperspectral CART classification of *E. esula*.

Centaurea maculosa

Multispectral Imagery. Using the strictest interpretation of accuracy, user's accuracy for *C. maculosa* was 45%, user's accuracy for vegetation was 73%, overall accuracy was 48%, and the Khat value was 0.06 for the classified map (Table 3). Similar to the *E. esula* site, vegetation was confused with the target weed, and the resulting map visually revealed indiscriminant and wide scattering of *C. maculosa*, indicating substantial overclassification (Figure 2). There appeared to be no apparent pattern to the *C. maculosa* distribution. As the thresholds became less stringent, overall accuracy, user's accuracy for *C. maculosa*, and Khat values increased until a maximum Khat value of 0.33 was reached at the 35% threshold (Figure 4). User's accuracy for vegetation increased until the 10% threshold, and then declined as the rules for weed polygons became stricter, thus causing more confusion of weed polygons for associated vegetation. At the 45% threshold, overall accuracy peaked at 68% and user's accuracy for *C. maculosa* reached 69%. Khat again reached a maximum of 0.33 at the 45% threshold.

Hyperspectral Imagery. Using the strict interpretation of accuracy for the CART classified map, user's accuracy for *C. maculosa* was 74%, user's accuracy for vegetation was 62%, overall accuracy was 65%, and the Khat value was 0.28 (Table 3). The map revealed scattered infestations of *C. maculosa* throughout the site, with larger and denser infestations around Virginia City and in the proximity of mining sites (Figure 2). Increasing the threshold caused very little change in overall accuracy and user's accuracy for vegetation (Figure 4). User's accuracy for the target weed increased as less commission errors were made with vegetation. As thresholds for vegetation became incrementally less strict, more vegetation polygons were correctly classified and not confused with *C. maculosa*. At the 25% threshold, user's accuracy for *C. maculosa* increased to 86% and overall accuracy peaked at 67%.

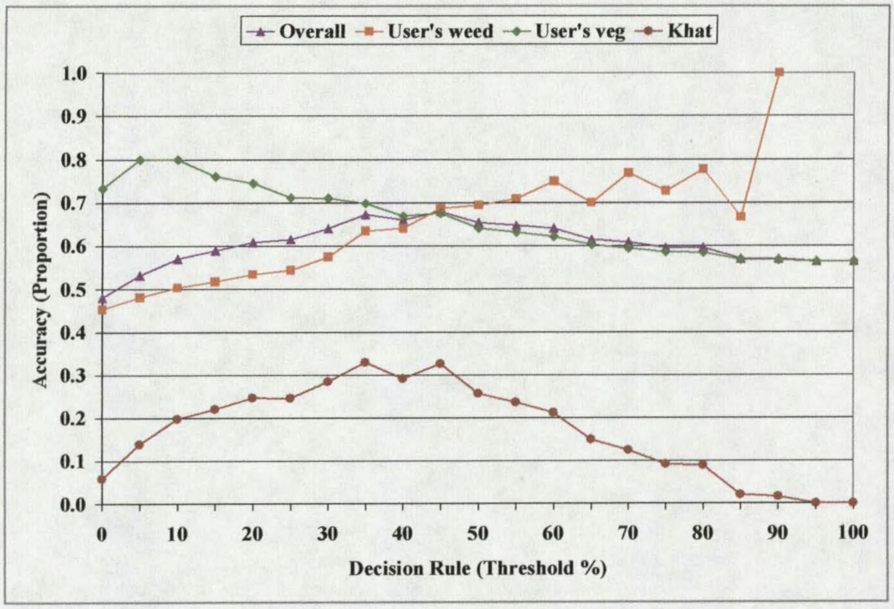

(a)

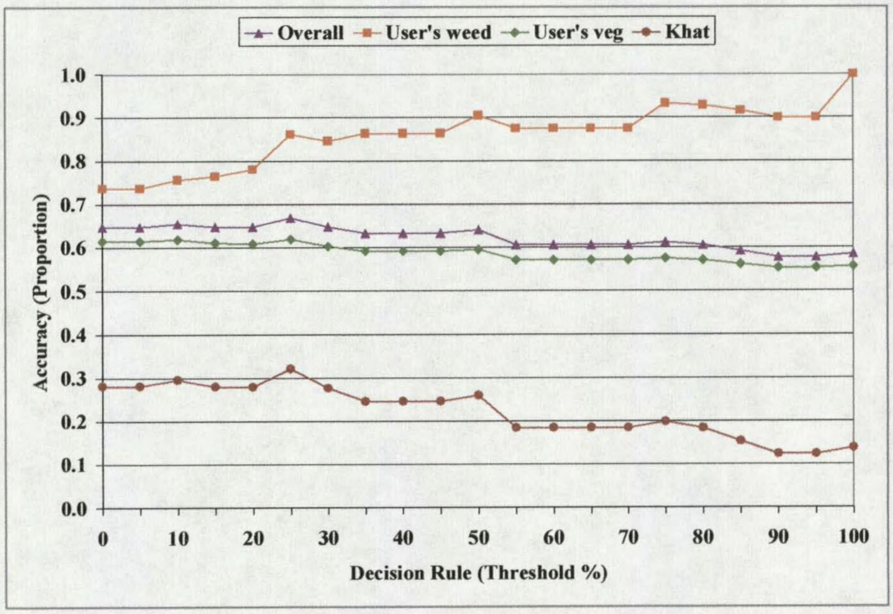

(b)

Figure 4. Accuracy assessment curves comparing incremental decision rules for (a) multispectral ML classification and (b) hyperspectral CART classification of *C. maculosa*.

Discussion

Visually, the maps were different; the hyperspectral CART classifications more adequately reproduced the ecological and dispersal behavior of both invasive species. We can make no statistical claim, however, that hyperspectral CART imagery produced more accurate maps of the invasive plants than multispectral ML imagery because we could not use Kappa in a Z test to compare classifications. Instead, we examined user's accuracy for the target weed species as an unbiased estimate of map reliability for that particular class. A comparison of summary measures and classified maps is justified and in keeping with our objectives. What do the different map accuracies impart about the utility of employing such remote mapping methods for monitoring invasive plant populations? How reliable are the resulting weed maps? Are the maps appropriate for use at management scales?

Comparisons: Imagery, Algorithms, Invasive Plant Species

User's accuracy, or the proportion of locations for which the map label is correct on the ground, has been defined as the usefulness or reliability of the map (Aronoff 1982, Janssen and van der Wel 1994) and is arguably of most practical interest to a resource manager. The hyperspectral CART system produced higher user's accuracies for both *E. esula* and *C. maculosa*. The hyperspectral imagery at 5 m spatial resolution classified with the CART algorithm produced the highest overall Khat value (0.32) and the highest user's accuracy (61%) for *E. esula* of each classified image at the strict interpretation of accuracy. The hyperspectral CART classification resulted in a 20% increase in weed user's accuracy over the multispectral classification (41%). While recommending a hyperspectral CART classification for *E. esula* over the multispectral ML classification could not be statistically proven by comparing Khat statistics, the higher user's accuracy for the hyperspectral CART map indicated a manager might find *E. esula* on the ground more consistently than with the multispectral ML map. The estimates of Kappa and user's accuracies for the two classifications were substantially different, and, with regard to environmental patterns revealed by the maps, the classifications were different visually.

Similar to the *E. esula* classifications of the hyperspectral CART and multispectral ML combinations, the hyperspectral CART system resulted in a higher overall Khat value (0.28) and a higher user's accuracy for *C. maculosa* (74%) at the strict interpretation of accuracy. The hyperspectral CART classification resulted in a 29% increase in weed user's accuracy over the multispectral ML classification (45%). Visually the maps were different and the hyperspectral CART map was qualitatively more representative of the *C. maculosa* infestations at the site. User's accuracy for *C. maculosa* was nearly 30% higher for the hyperspectral CART map than the multispectral ML map, and such a measure might be significant to a manager interested in monitoring plant distributions.

<u>Reflectance Characteristics of *E. esula*</u>. Although healthy vegetation exhibits similar reflectance properties, differentiation is possible due to structural characteristics, leaf area and geometry, surface construction, water content, and, in the VIS spectral range, pigmentation (Knipling 1970, Woolley 1971). Structural characteristics and leaf

area/geometry interact with shading and background reflectances, further increasing spectral separation. Successful classification of imagery by an algorithm can be dependent on physiological and phenological variability of the invasive plants and associated vegetation (Lass and Callihan 1997).

E. esula primarily spreads through rhizomatous rootstalks (Lajeunesse et al. 1999), thus, once established, can aggressively grow in dense patches that ultimately exclude native vegetation. In some instances, a resilient and healthy native community can prevent total exclusion of resources by *E. esula*, in which case the weed coexists in moderate density infestations with native vegetation (Sheley et al. 1996). During flowering, bright yellow-green bracts branch and form a dense and complex-angled upper canopy. This combination of growth-habit and structural characteristics determines reflectance characteristics and how spectrally distinct *E. esula* might be. In our study, *E. esula* patches of varying percent cover were mixed with native vegetation. In addition, some *E. esula* plants had begun to senesce. Training polygons exhibited a high degree of variability. CART applied to the hyperspectral imagery might have best compensated for the variability to produce the most accurate results. While we could not isolate any single variable in the combination of spectral resolution, spatial resolution, and algorithm as being most influential for producing higher accuracies (for example, higher *E. esula* user's accuracies of the hyperspectral system might have been a result of decreased spatial resolution or an interaction of all three variables), understanding of how CART and ML algorithms function allows insight into the results.

CART examined all 128 spectral bands, but focused on those spectral bands that ultimately provided most separability by reducing deviance in the final clusters.

Although there might have been higher class confusion in certain bands, CART would have disregarded those bands if they did not reduce deviance effectively.

The maximum likelihood classifier used with the multispectral imagery calculated probability density functions (PDF) from *E. esula* and vegetation training samples using spectral response in the 4 bands. Probability of an unknown pixels membership to a given cluster was calculated based on PDF variance and distance to mean. Given the variability in percent cover and phenology of the *E. esula* training polygons, the PDF for the weed class potentially resulted in high covariance and overlap with vegetation (Lillesand and Kiefer 2000).

Reflectance Characteristics of *C. maculosa*. Understanding the ecology and growth habit of *C. maculosa* provides information about potential spectral separation of *C. maculosa* from other vegetation. *C. maculosa* flowers are purple to pink and borne on single or branching flowerheads on multiple stems. A single plant produces between 25 –35 flowers (Sheley et al. 1999a). Unlike *E. esula*, which blooms early in the growing season in the north, *C. maculosa* plants have wide flowering amplitude, blooming from June to October. It would be difficult to characterize a stand of *C. maculosa* using remote sensing based solely on phenology, unless the stand happened to be flowering uniformly. Studies have documented increased soil exposure on sites dominated by *C. maculosa* over sites with a greater diversity of perennial species (Tyser and Key 1988, Lacey et al. 1989). In arid and semi-arid environments where vegetation cover is reduced and the soil percentages are greater, researchers have modeled the increasing influence of soil reflectance in separating scene components (Graetz and Gentle 1982, Smith et al. 1990, Roberts et al. 1993, Ustin et al. 1996). Areas dominated with *C. maculosa* and with reduced vegetation understory and increased bare ground will reflect light differently than areas with a diverse and multi-storied ground cover.

In general, soil has a flatter spectral response curve with fewer absorption features than photosynthetically active vegetation and has higher reflectance in the VIS and lower reflectance in the NIR (Lillesand and Kiefer 2000). CART will capitalize on variable brightness patterns by using the bands that emphasize differences in the process of clustering. The hyperspectral CART classification of *C. maculosa* was different from the other classifications in that it produced a higher user's accuracy for the target weed (74%) than for vegetation (62%) at the 0% threshold. Further, the hyperspectral CART system produced the highest user's accuracy for *C. maculosa* of all algorithms and imagery.

Management Implications

The Montana Noxious Weed Survey and Mapping System (MNWSMS) describes accuracy levels for ground-based invasive plant mapping using estimated attribute accuracy and horizontal accuracy (Table 4) (Cooksey and Sheley 1998b). Workers performing ground-based mapping were to use the MNWSMS metadata form to estimate their accuracy based on three levels before entering spatial data into a statewide database.

Table 4. Accuracy levels for ground-based mapping invasive plants from the Montana Noxious Weed Survey and Mapping System's metadata form (Cooksey and Sheley 1998a).

Accuracy Level	Factors that Determine Accuracy
Level I	Attribute accuracy = 80 – 100% Horizontal accuracy = 0-20 m
Level II	Attribute accuracy = 60 – 80% Horizontal accuracy = 20 – 100 m
Level III	Attribute accuracy < 60% Horizontal accuracy > 100m

The multispectral classifications of both *E. esula* and *C. maculosa* at the 0% threshold produced map accuracies comparable to Level III of ground-based invasive plant maps. For both invasive plants, over half of the mapped weed locations were false positives and, according to our estimate of the population, these areas were not truly infested in the field. By moderating the decision rules and relaxing the thresholds, user's accuracies for both weed species peaked around the 50% threshold and ranged from 41 – 84% for *E. esula* and from 45 – 69% for *C. maculosa* (Figures 3 and 4). If a manager wanted to be more certain the proportion of sites visited would indeed contain weed infestations, they might consider looking only at mapped areas with greater than 50% weed pixels. For *E. esula* the improvement was greatest: 84% of areas showing more than 50% weed pixels would truly contain infestations in the field, a much more efficient use of time than had only 41% of the sites contained *E. esula* plants. In relaxing the decision rules, thresholds increase the user's accuracy of the multispectral imagery, however, producer's accuracy for *E. esula* decreases as weed thresholds increase and more omission errors occur. The multispectral imagery was easier and less time-consuming to process and can be more accurately georegistered, ultimately saving costs when using the imagery to map invasive plants. The multispectral ML maps were not accurate enough to use in a site-specific manner, or to locate small outlying infestations, but they might be used to locate areas of potential infestations such as drainages or midslopes.

The hyperspectral CART classifications of both *E. esula* and *C. maculosa* provided user's accuracies close to Level I of ground-based invasive plant mapping methods at the strictest accuracy threshold. Again, relaxing decision rules by allowing an incrementally higher percentage of non-category pixels present in each accuracy assessment polygon increased weed user accuracies. This translated into a map that accepted a certain percentage of weed pixels in areas classified as vegetation, and required a minimum percentage of weed pixels in areas classified as weed.

The minimum mapping unit of the hyperspectral imagery was the 3 – 5 m resolution cell size. The CART algorithm was not designed to locate weed patches smaller than the minimum mapping unit. Spectral mixture analysis might have detected infestations smaller than the resolution cell size, however, we chose to test algorithms that required less complex training site selection.

Although at a preferable resolution for monitoring small spatial patterns of invasive plants, the multispectral imagery proved less reliable at accurately detecting infestations. While not of a resolution capable of detecting single plants, the resolution of the hyperspectral imagery was nevertheless at a management scale that might permit early detection of small, outlying infestations. Further, this study has shown that classification of 3 - 5 m resolution hyperspectral imagery was of accuracy suitable for mapping invasive plant infestations at landscape scales.

Limitations

While the hyperspectral CART classifications performed adequately, intensive inventory using traditional ground based mapping methods, though perhaps more time-consuming, is generally capable of providing more accurate weed distribution data (Cooksey and Sheley 1998b). Potential factors contributing to inaccuracies include sources of spatial error and limitations of the training and reference sample data. Due to spatial accuracy limitations imposed by imperfect georegistration, it is theoretically impractical to locate infestations less than the size of the minimum mapping unit or resolution cell size (Aronoff 1985). In theory, we could not expect to locate accurately weed infestations smaller than 1 m^2 for the multispectral imagery, and 5 m^2 for hyperspectral imagery. In reality, we were further constrained by the +/-6 m accuracy of the DOQ to which the imagery was registered (USGS 2001), by the accuracy of the GPS receivers, and by errors introduced through visually estimating the location of the hyperspectral reference samples. Limitations in the sample data include wide phenological variability in the class training samples, small polygon area, and inference beyond the mean polygon size of the training samples.

The training samples for both target weed and vegetation undoubtedly captured a wide variety of reflectance ranges due to variable percent cover and species diversity. Our intent was to capture a certain degree of natural variability within the classes and thus to represent dynamic environmental circumstances such as different stages of invasion, a diverse understory, and variable shade and illumination conditions (Walsh 1987). The error matrices and maps, however, consistently revealed overclassification of the target weed. There was significant confusion of weed-free vegetation with target weeds at both study sites. This indicated that the training data did not effectively narrow the range of spectral variability for each class to avoid overlap. Utilizing low-density weed patches as training samples, and therefore diluting the weed spectral response with vegetation spectral response, most likely contributed to the spectral overlap. A potential solution to the problem of non-homogeneity of the training samples is to apply spectral unmixing to model the fractions of vegetation, target weed, soil, and shade (Adams et al. 1993, Roberts et al. 1993, Okin et al. 2001).

Another source for potential error occurred by inferring beyond the training data, or extending spectral signatures beyond their true spatial extent (Jensen 1996). For example, at the *E. esula* site, we did not sample the hay meadow in the southeast portion of the map and the vegetation spectral response was not represented for this area. To compensate for this gap in reference data we chose to mask the hay meadow out of the study area. In retrospect, a stratified sampling design that identified and sampled common and distinct associated vegetation types in the study area might have provided more representative reference data.

Another limiting factor that was exacerbated for the hyperspectral imagery was the relatively small polygon size, which resulted in a low number of pixels representing the training samples. With an increase in resolution cell size from 1 square meter for the multispectral imagery to 9 or 25 square meters for the hyperspectral imagery, the average number of pixels per weed polygon decreased from 68 to 5 pixels for the *C. maculosa* site and from 90 pixels to 3 pixels for the *E. esula* site. The reduced sample size did not provide a representative sample of the landscape. In statistical classifiers, a better estimate of the mean and covariance matrix is achieved with a greater sample size (Lillesand and Kiefer 2000). We were unable to collect larger polygons of the target weeds.

There were definite lessons learned from this study based on (1) remote sensing issues and (2) invasive plant density/phenology issues. The remote sensing lessons largely revolved around imagery, classification method, and ground reference samples. The hyperspectral imagery was not easily rectified. We mitigated the registration issues by hand-locating the reference samples, but this undoubtedly impacted the operability and the accuracy. Methods for rectifying hyperspectral imagery are available at greater expense. In addition, hand mapping onto imagery while in the field can provide maximum locational accuracy (Aspinall In press). Unfortunately, the imagery was not available at the time of sampling.

The classification algorithms we applied were those that had proven utility in other applications. Part of the objective was to use imagery and processing/analysis methods that were operationally practical. The ML classifier is commonly used with multispectral imagery (Lillesand and Kiefer 2000) and CART has seen relative success with hyperspectral imagery (Lawrence and Labus In press). The ML classification did not perform well with the classification scheme we used. The ground reference samples incorporated a large amount of spectral variability, potentially resulting in substantial overlap in the spectral signature between target weed and associated vegetation. Larger infestations with consistently higher weed density might have increased spectral separability and reduced the variability of the target weed spectral response.

The density of *E. esula* and *C. maculosa* at both sites were not 100% cover or exclusive of other plants, thus we did not capture pure target weed reflectance with the reference samples. Timing image capture with peak flowering, though logistically not always possible, might also have mitigated the high variability of weed spectral response. *E. esula* exhibited wide phenology, increasing the variability of spectral response.

Even with the limitations, this study provided valuable information about applying airborne digital imagery to mapping invasive species. Operational and practical methods were applied to classify multispectral and hyperspectral imagery. Multispectral ML and hyperspectral CART classifications produced different distribution maps of the target weeds. User's accuracy was used as a measure of map reliability to compare multispectral ML and hyperspectral CART classifications. The hyperspectral CART classifications resulted in higher user's accuracy for both *E. esula* and *C. maculosa.* Though not of sufficient accuracy to detect small outlying infestations that are critical to eradicate in order to slow the spread of invasive plants, the hyperspectral imagery provided results with user's accuracies similar to intensive hand-mapping methods. Given the time and cost required to perform intensive ground surveys, the tradeoff of lower accuracy might be worthwhile in situations where an estimation of infestation distributions over large areas will assist with invasive plant management objectives.

CHAPTER 4

EFFECTS OF COLOR BALANCING OF AIRBORNE MULTISPECTRAL IMAGERY ON INVASIVE PLANT MAPPING

Introduction

Airborne digital sensors with spatial resolution comparable to resolution achieved with aerial photography have become widely commercially available. One example of a high spatial resolution sensor is Positive Systems' Airborne Data Acquisition and Registration (ADAR) 5500 system, which can produce a spatial resolution of between 0.5 and 1 m at lower altitudes (Lass et al. 1996, Phinn et al. 1996, Phinn et al. 1999). With an increase in ground resolving power 30 linear times traditional satellite sensors such as Landsat, these high spatial resolution sensors might improve the accuracy of classifying vegetation to the species level. A study was initiated to classify ADAR 5500 imagery for two species of invasive plants in rangeland environments of southwestern Montana and to determine the classification accuracy. However, while mosaicking individual scenes into one composite image brightness gradients were observed within and between scenes that resulted from interaction of sun-sensor geometry (Figure 5). Acknowledging that modeling the mechanistic and physical principles causing the bidirectional reflectance was beyond the scope of the project, we tested the effect that Positive Systems' Digital Imaging Made Easy (DIME^{TM}) color balancing software had on mitigating the brightness gradient and changing classification accuracy results from non-color balanced imagery.

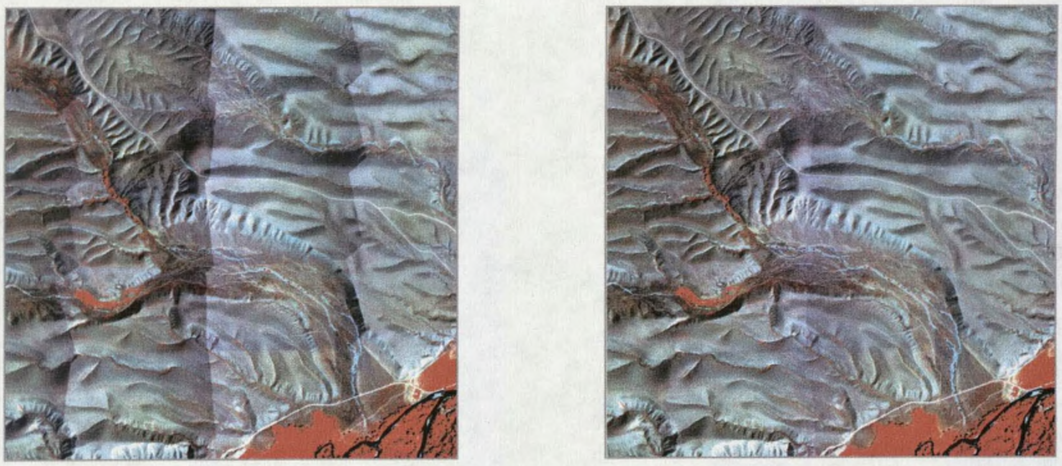

(a) (b)

Figure 5. Mosaicked ADAR 5500 image of *E. esula* site captured on 7 August 1999 in Madison County, Montana showing (a) within and between scene brightness gradients and (b) after processing with DIME^{TM} color balancing software. Bands 4 (780-920 nm), 3 (610-700 nm), and 2 (520-610 nm) are displayed as red, green, blue, respectively.

Background: Causes of Reflectance Anisotropy

Extracting quantitative information about land cover such as biophysical or structural characteristics, community composition, or taxonomic discrimination to the species level is an increasingly important objective of remote sensing (Graetz 1989). Interpreting features using spectral or structural information from reflected light, however, can be complicated by brightness gradients within image scenes that result from reflectance anisotropy. These illumination differences can result from several factors, including the interaction of illumination geometry (solar elevation and azimuth) and sensor geometry (view angle) (Royer et al. 1985), differential atmospheric scattering, exposure falloff, vignetting effects, and specular reflection (Lillesand and Kiefer 2000). Such brightness variations have potential to significantly mask the spectral variations between objects.

The intrinsic variability of directional reflectance from earth surfaces has been widely researched and documented (Irons et al. 1986, Walthall 1997). Bidirectional reflectance results from the interaction of two directions: one direction viewing and one direction illuminating the target (Norman et al. 1985). Further complicating matters, bidirectional reflectance is spectrally dependent, varies with the length of atmospheric path, and varies with cover type, thus making it difficult to model (Royer et al. 1985, Pickup et al. 1995).

The interaction of sensor and sun angle geometry causes significant brightness gradients in airborne digital imagery or in satellite imagery with large scan angles or side-looking capability (Royer et al. 1985). For example, many sensors utilize scanners in which the sun-sensor geometry changes for each pixel scanned, thus compounding brightness gradients at wide look angles. As a result, many researchers have focused their efforts on developing methods for normalizing within-scene radiometric variability. Such methods include physically based bidirectional reflectance distribution function (BRDF) models (Norman et al. 1985), empirically based corrections that model distortions (Royer et al. 1985, Pickup et al. 1995, Kennedy et al. 1997, Walthall 1997), and the use of band ratios (King 1991, Pickup et al. 1995, Qi et al. 1995).

Complex models that incorporate the physical parameters contributing to bidirectional reflectance, such as illumination and view angle geometry, wavelength, atmospheric attenuation, soil reflectance, vegetation type and density, leaf angle orientation, and canopy transmittance, have been developed (Norman et al. 1985, Irons et al. 1986). Such model parameters require intensive measurements and computations that are impractical or beyond the scope of many remote sensing objectives. Because of such research, some fundamental geometric properties of BRDF models have been successfully transferred to simplified empirical models (Norman et al. 1985, Royer et al. 1985, Irons et al. 1986, Pons and Sole-Sugraines 1994, Walthall 1997). Some researchers have measured success of a correction model through marked visual improvement of the imagery and preservation of the between-band spectral shapes (Kennedy et al. 1997). Others, with classification of land cover as their main goal, have used improved classification accuracy as the final measure of correction success (Pons and Sole-Sugraines 1994).

The overall objective of this study was to classify ADAR 5500 imagery for two invasive species of rangeland weeds. Further, from a practical invasive plant management standpoint, the study was implemented to determine if methods utilizing remote sensing for mapping noxious weeds over large rangeland areas were operationally and logistically feasible. To streamline and maintain simplicity of image preprocessing, we did not attempt to model the bidirectional parameters contributing to image anisotropy. Rather, our immediate objective was to test the effect of color balancing on mitigating the brightness variations and how such an approach impacted the classification accuracy.

Methods

Imagery

The imagery was obtained using the ADAR 5500 sensor, an electronic imaging instrument that consists of four cameras with 20 mm lenses that are individually filtered to record reflectance over the ranges 460 – 550 nm, 520 – 610 nm, 610 – 700 nm, and 780 – 920 nm. The four bands were coregistered by PSI. The spatial resolution of the imagery was 1 m.

Study Sites

The imagery covered two sites in Madison County, Montana, each site approximately 1,024 ha in area (Figure 1). The first site was flown on 7 August 1999 from 10:45 am to 11:06 am Mountain Daylight Time (MDT). Vegetation at this site consisted primarily of a mixture of rangeland grasses and shrubs with moderate invasion of *Euphorbia esula* L. (leafy spurge), a rhizomatous perennial introduced from Eurasia. The *E. esula* site was located at the southern end of the Highland Mountains and the predominant physiography consisted of dissected upland fans and terraces of the Big Hole River. *E. esula* primarily occupied drainage bottoms and surrounding hillsides and was distributed with native vegetation in low to high density patches of infestation. The landscape and land cover at the *E. esula* site was relatively uniform and homogeneous.

The second site was flown on 10 August 1999 from 10:55 am to 11:17 am MDT. Vegetation at this site was primarily mixed forest-rangeland with moderate invasion of

Centaurea maculosa Lam. (spotted knapweed), a taprooted perennial also introduced from Eurasia. The *C. maculosa* site was located north of the Gravelly Range and the physiography consisted of upland hills and ridges and floodplains of perennial streams. *C. maculosa* occurred throughout the site with no obvious pattern of distribution and mixed with native vegetation in low to high density patches of infestation. This area was heavily mined in the 1800s, and the landscape bore signs of mining disturbance such as roads, tailings piles, mineshafts, buildings, and equipment. The landscape and land cover at the *C. maculosa* site was more diverse than the *E. esula* site and consisted of greater topographic relief and mixed physiognomy of grasses, shrubs, and trees.

Image Processing

Imagery was georeferenced to digital orthophoto quadrangles (DOQ) and color balanced using PSI's proprietary DIME^{TM} software. Two images were classified for each site: one image was georeferenced only, with no color balancing applied, and another image was georeferenced with color balancing applied. Images were classified with ERDAS Imagine software using a maximum likelihood (ML) classifier.

Reference samples of the target weed (*E. esula* or *C. maculosa*) and associated vegetation were field collected in August 1999 using Trimble GeoExplorer II Global Positioning System (GPS) receivers. The GPS field data were differentially corrected. The reference samples were split into two sets; (a) image reference spectra for the ML algorithm and (b) ground reference samples for the accuracy assessment. To obtain image reference spectra, image statistics were extracted using Imagine software for use in the ML classifier. The classification scheme consisted of two classes: the target weed and associated vegetation. For each site, identical training and accuracy assessment polygons were used so that the differences in results were based solely on the result of color balancing.

Analysis

An accuracy assessment was performed in which the GPS ground reference polygons were compared to the image classification. Error matrices were created for the four classified images, and overall accuracy, producer's accuracy, and user's accuracy were calculated. In addition, a Kappa analysis was used to compute a Khat statistic and a variance of Khat. The Khats were used in a two-tailed Z test to determine if there were statistically significant differences between the color balanced and non-color balanced error matrices. Differences in Khat values indicate differences in the level of agreement between classification and ground truth for two different classifications (Congalton and Green 1999).

The sample units used for the accuracy assessment were polygons. Because the strictest interpretation of correctly classified vegetation and weed polygons was unrealistic for a discrete thematic map (weed infestations were generally not 100% infested), fuzzy decision rules for determining whether a given reference polygon overlaid on the pixelized classification map was correctly classified followed incremental percentage thresholds. For example, in the strictest interpretation, or 0% threshold, no weed pixels would be allowed in the vegetation polygons in order to be correctly classified, while one weed pixel in a polygon of vegetation pixels would constitute correct classification for weed polygons. Accuracy thresholds were calculated at 5% increments. At the 50% threshold, a vegetation polygon was allowed 50% of total pixels to be weed pixels, while a weed polygon was required to have at least 50% weed pixels.

Results

Accuracy Assessment

Strict Decision Rule. Using the strictest interpretation of accuracy (0% threshold), at the *E. esula* site overall accuracy was 50% for both the color balanced and non-color balanced imagery (Table 5), and there was no significant difference between Khat values (p–value = 0.95). For the color balanced imagery, a Khat statistic of 0.14 was observed, a slightly higher accuracy than the non-color balanced imagery. These results indicated that there was not significantly better agreement between the classification and ground truth for the color balanced imagery than for the non-color balanced imagery. For both color balanced and non-color balanced imagery, the user's accuracy for *E. esula* was 41%. From a management perspective, user's accuracy provides the most valuable information about the classification accuracy or effectiveness of the map because it indicates the proportion of *E. esula* pixels on the map at which a map user would actually find *E. esula* on the ground.

Table 5. Summary measures from confusion matrices for classified maps of *E. esula* using the 0% threshold (strict) decision rule. Non-color balanced and color balanced classifications are compared.

Non-Color Balanced Imagery 0% Threshold			**Color Balanced Imagery 0% Threshold**		
%	*E. esula*	Vegetation	%	*E. esula*	Vegetation
User's	41	82	User's	41	83
Producer's	90	27	Producer's	90	28
Overall	50		Overall	50	
Khat	0.13		Khat	0.14	

Similarly, using the strictest rules, an accuracy assessment for the *C. maculosa* site revealed slightly higher overall accuracy for the color balanced imagery (Table 6) but no statistically significant differences in the Khat values (p–value = 0.81). While the Khat value for the color balanced imagery was higher than the Khat value for the non-color balanced imagery, the user's accuracy showed very little difference. Approximately 45% of either classified map's pixels in truth would contain *C. maculosa* in the field.

Table 6. Summary measures from confusion matrices for classified maps of *C. maculosa* using the 0% threshold (strict) decision rule.

Non-Color Balanced Imagery 0% Threshold			**Color Balanced Imagery 0% Threshold**		
%	*C. maculosa*	Vegetation	%	*C. maculosa*	Vegetation
User's	44	60	User's	45	73
Producer's	91	10	Producer's	94	13
Overall	46		Overall	48	
Khat	0.01		Khat	0.06	

30% Threshold Decision Rule. The error matrices for color balanced and non-color balanced classifications were also compared at 30% thresholds. At the 30% threshold, the Khat values were close to maximized, indicating best agreement between classification and reference. We acknowledged that by using the threshold approach an increasing level of misclassification within a polygon was accepted. The threshold rule results, however, are useful for management purposes because if accuracy levels are high a manager would not expect to find *E. esula* where resulting map showed less than 30% weed pixels. Using the maximized accuracy or best threshold would allow the manager to target areas most likely infested with the invasive plant.

At the *E. esula* site, Khat values at the 30% threshold improved over the strict decision rule for the color balanced and non-color balanced imagery (Table 7). Overall accuracy for the color balanced image and non-color balanced image was estimated to be 74% and the Khats were not significantly different (p–value = 0.94). Similar to results from the strict decision rule, the Khat statistic was slightly higher for the color balanced image, as was the user's accuracy.

At the *C. maculosa* site, Khat values at the 30% threshold also improved over the strict decision rule for the color balanced and non-color balanced imagery (Table 8). In contrast to the *E. esula* site, however, the Khat decreased slightly with color balancing, though not significantly (p–value = 0.98). Overall accuracy was also slightly lower for the color balanced image and the user's accuracy decreased by 4% from the non color-balanced image to the color balanced image.

Table 7. Summary measures from confusion matrices for classified maps of *E. esula* using the 30% threshold decision rule.

Non-Color Balanced Imagery 30% Threshold			**Color Balanced Imagery 30% Threshold**		
%	*E. esula*	Vegetation	%	*E. esula*	Vegetation
User's	64	79	User's	66	79
Producer's	63	80	Producer's	60	82
Overall	74		Overall	74	
Khat	0.43		Khat	0.44	

Table 8. Summary measures from confusion matrices for classified maps of *C. maculosa* using the 30% threshold decision rule.

Non-Color Balanced Imagery 30% Threshold			**Color Balanced Imagery 30% Threshold**		
%	*C. maculosa*	Vegetation	%	*C. maculosa*	Vegetation
User's	62	68	User's	58	71
Producer's	54	74	Producer's	68	61
Overall	65		Overall	64	
Khat	0.29		Khat	0.28	

Discussion

The goal of spectral classification is to discriminate between classes of interest based on how those classes reflect electromagnetic energy differently. Land cover classes can be a heterogeneous mix of community types such as mixed deciduous forest or a homogeneous group as when classifying to species level, but these unique classes are presumed to be separable from other scene components (Foody 1988). Spectral separability, however, is often masked by reflectance anisotropy, which is spatially dependent and increases the spectral variability of classes. Methods for mitigating this anisotropy include modeling sun-sensor-object geometry, which has been shown to preserve spectral shape (Kennedy et al. 1997), or band ratioing, which does not preserve spectral values. We determined that color balancing did not significantly improve or reduce classification accuracy.

While DIME™ color balancing visually provided improvement (Figure 5) and in most cases slight (non-significant) improvement in estimated classification accuracies, it did not provide statistically significant differences between classifications. One possible reason for no statistically significant difference was that the sample sizes (n = 133 for *E.*

esula, n = 156 for *C. maculosa*) were not of sufficient power to detect differences, although we do not know of a statistical power test of the Khat Z test. When pixels were used as the accuracy assessment sample unit, increasing sample size one-hundredfold, significant differences were detected between error matrices for color balanced and non-color balanced imagery, but the color balanced images were significantly less accurate. For this study, however, the pixel was not a biologically meaningful sampling unit; noxious weeds are distributed across the landscape in patches of varying density.

DIME™ color balancing is proprietary software that smoothes contrasts, minimizes brightness differences, and is promoted to create seamless mosaics. As such, color balancing is mainly used for visual enhancement and should be approached cautiously for a more specific processing goal. The specific modeling techniques employed in DIME™ software are proprietary. In general, color balancing models brightness variations by attempting to fit a general trend through a surface of variation in digital number (DN). DN values are transformed based on the type of surface fitted to the brightness variation. Physical, atmospheric, and topographic variables that might affect radiometric differences are not directly modeled. While offering visual improvement, color balancing might not preserve unique spectral features that contribute to class spectral separability. When applying color balancing, low amplitude spectral features might become entirely masked or the distance between means for classes with higher variances might become insignificant.

The training polygons used as image spectra represented natural infestation conditions and thus were not pure weed spectra. Polygons contained varying densities of the target weed mixed with other vegetation, surface litter, soil, substrate, and shade. The overlap between target weed and associated vegetation clusters might have been increased with color balancing, resulting in greater class confusion.

DIME™ color balancing is a processing technique that can be readily applied to commercially available ADAR 5500 imagery. While visually improving reflectance anisotropy within mosaicked images, DIME™ also resulted in slightly higher estimated classification accuracies. A comparison of Khat values, however, showed there was no significant difference in classification accuracy between imagery that was color balanced with DIME™ and imagery that was not color balanced.

CHAPTER 5

SUMMARY

Two airborne digital imaging systems were examined to assess their practical utility in mapping two invasive rangeland species. Multispectral imagery (4-band) with spatial resolution of 1 m was classified with a ML algorithm. Hyperspectral imagery (128-band) with spatial resolution of 3 and 5 m was classified with CART analysis and a SAM algorithm.

Results of the multispectral ML classification indicated that both *E. esula* and *C. maculosa* had lower accuracies than intensive ground-based survey methods (Level I) developed by the Montana Noxious Weed Survey and Mapping System (MNWSMS) (Cooksey and Sheley 1998b). Overall accuracy for both sites were less than or equal to 50% and user's accuracies for *E. esula* and *C. maculosa* were less than 50%. Relaxing the accuracy assessment decision rules for classifying target weed or vegetation produced user's accuracies up to 84% for *E. esula* and 69% for *C. maculosa.* Maps derived from the multispectral classification methodology applied in this study should be used to explore general areas most likely infested by target weeds and should not be used in a site-specific manner.

Results of the hyperspectral SAM classification indicated that both *E. esula* and *C. maculosa* had accuracies less than MNWSMS intensive ground-based survey methods. The SAM classification of *C. maculosa* was essentially no better than a random classification according to a Kappa analysis, and as a result, the accuracies were significantly lower than the hyperspectral CART system. The SAM classification methodology we applied does not provide accurate invasive plant infestation information.

Results of the hyperspectral CART classification indicated that both *E. esula* and *C. maculosa* maps achieved accuracies comparable to moderate MNWSMS ground-based mapping accuracy levels (Level II). Differences in user's accuracy and in the resulting map indicate that the hyperspectral CART system produced substantially higher accuracies and more realistically represented infestation patterns. User's accuracy for the hyperspectral CART system was 20% higher for *E. esula* and 29% higher for *C. maculosa* than the multispectral ML system.

Neither the multispectral nor the hyperspectral system was able to detect small outlying infestations with reliability, however, methodologies for mapping landscape-scale areas were shown to provide accuracies similar to moderate MNWSMS levels achieved through ground-based mapping. The results of this study offer alternative methodologies for mapping extensive areas that, combined with more intensive ground-based mapping of local areas, can provide both generalized and specific infestation data at management scales.

REFERENCES CITED

Adams, J. B., M. O. Smith, and A. R. Gillespie. 1993. Imaging spectroscopy: Interpretation based on spectral mixture analysis. Pages 145-166 *in* C. M. Pieters and P. A. J. Englert, editors. Remote Geochemical Analysis: Elemental and Mineralogical Composition. Cambridge University Press, Cambridge.

Anderson, G. L., J. H. Everitt, D. E. Escobar, N. R. Spencer, and R. J. Andrascik. 1996. Mapping leafy spurge (*Euphorbia esula*) infestations using aerial photography and geographic information systems. Geocarto International 11:81-89.

Anderson, G. L., J. H. Everitt, A. J. Richardson, and D. E. Escobar. 1993. Using satellite data to map false broomweed (*Ericameria austrotexana*) infestations on south Texas rangelands. Weed Technology 7:865-871.

Anderson, J. R., E. E. Hardy, J. T. Roach, and R. E. Witmer. 1976. A land use and land cover classification system for use with remote sensor data. Professional Paper 964, US Geological Survey, Washington DC.

Aronoff, S. 1982. Classification accuracy: A user approach. Photogrammetric Engineering and Remote Sensing 48:1299-1307.

Aronoff, S. 1985. The minimum accuracy value as an index of classification accuracy. Photogrammetric Engineering and Remote Sensing 51:99-111.

Aspinall, R. J. In press. Use of logistic regression for validation of maps of the spatial distribution of vegetation species derived from high spatial resolution hyperspectral remotely sensed data. Ecological Modelling.

Bangsund, D. A., J. F. Baltezore, J. A. Leitch, and F. L. Leistritz. 1993. Economic impact of leafy spurge on wildland in Montana, South Dakota, and Wyoming. Agricultural Experiment Station, North Dakota State University, Fargo.

Bangsund, D. A., F. L. Leistritz, and J. A. Leitch. 1999. Assessing economic impacts of biological control of weeds: The case of leafy spurge in the northern Great Plains of the United States. Journal of Environmental Management 56:35-43.

Boardman, J. W., and R. O. Green. 2000. Exploring the spectral variability of the earth as measured by AVIRIS in 1999. R. O. Green, editor. 2000 AVIRIS Airborne Geoscience Workshop, Pasadena, CA.

Boast, R. R., and R. G. Shelito. 1989. Soil Survey of Madison County Area, Montana. USDA, Soil Conservation Service.

Breiman, L., J. H. Friedman, R. A. Olshen, and C. J. Stone. 1984. Classification and Regression Trees. Wadsworth International Group, Belmont, CA. 358 pp.

Caldow, R. W. G., and P. A. Racey. 2000. Introduction: Large-scale processes in ecology and hydrology. Journal of Applied Ecology 37:6-12.

Carson, H. W., L. W. Lass, and R. H. Callihan. 1995. Detection of yellow hawkweed with high resolution multispectral digital imagery. Weed Technology 9:477-483.

Cihlar, J., D. Manak, and N. Voisin. 1994. AVHRR bidirectional reflectance effects and compositing. Remote Sensing of Environment 48:77-88.

Cochrane, M. A. 2000. Using vegetation reflectance variability for species level classification of hyperspectral data. International Journal of Remote Sensing 21:2075-2087.

Cohen, J. 1960. A coefficient of agreement for nominal scales. Educational and Psychological Measurement 20:37-46.

Congalton, R. G. 1991. A review of assessing the accuracy of classifications of remotely sensed data. Remote Sensing of Environment 37:35-46.

Congalton, R. G., and K. Green. 1999. Assessing the accuracy of remotely sensed data: Principles and practices. Lewis Publishers, Boca Raton. 137 pp.

Congalton, R. G., R. G. Oderwald, and R. A. Mead. 1983. Assessing Landsat classification accuracy using discrete multivariate analysis statistical techniques. Photogrammetric Engineering and Remote Sensing 49:1671-1678.

Cooksey, D., and R. L. Sheley. 1997. Noxious weed survey and mapping system. Rangelands 19:20-23.

Cooksey, D., and R. L. Sheley. 1998a. Mapping Noxious Weeds in Montana. EB148, Montana State University Extension Service, Bozeman, MT.

Cooksey, D., and R. L. Sheley. 1998b. Montana Noxious Weed Survey and Mapping System. MontGuide 9613, Montana State University Extension Service, Bozeman, MT.

Coulter, L., D. Stow, A. Hope, J. O'Leary, D. Turner, P. Longmire, S. Peterson, and J. Kaiser. 2000. Comparison of high spatial resolution imagery for efficient generation of GIS vegetation layers. Photogrammetric Engineering and Remote Sensing 66:1329-1335.

Deering, D. W., E. M. Middleton, and J. R. Irons. 1992. Prairie grassland bidirectional reflectance measured by different instruments at the FIFE site. Journal of Geophysical Research 97:18,887-818,903.

Dewey, S. A., K. P. Price, and D. Ramsey. 1991. Satellite remote sensing to predict potential distribution of Dyers woad (*Isatis tinctoria*). Weed Technology 5:479-484.

Dymond, J. R., J. D. Shepherd, and J. Qi. 2001. A simple physical model of vegetation reflectance for standardising optical satellite imagery. Remote Sensing of Environment 75:350-359.

Earth Search Sciences, Inc. 2002. Technology - About Probe-1. http://earthsearch.com/technology/frame_about_probe1.html.

ENVI. 1997. User's Guide. Better Solutions Consulting, Lafayette, CO. 377 pp.

Everitt, J. H., M. A. Alaniz, D. E. Escobar, and M. R. Davis. 1992. Using remote sensing to distinguish common (*Isocoma coronopifolia*) and Drummond goldenweed (*Isocoma drummondii*). Weed Science 40:621-628.

Everitt, J. H., G. L. Anderson, D. E. Escobar, M. R. Davis, N. R. Spencer, and R. J. Andrascik. 1995a. Use of remote sensing for detecting and mapping leafy spurge (*Euphorbia esula*). Weed Technology 9:599-609.

Everitt, J. H., and C. J. Deloach. 1990. Remote sensing of Chinese tamarisk (*Tamarix chinensis*) and associated vegetation. Weed Science 38:273-278.

Everitt, J. H., and D. E. Escobar. 1992. Airborne video systems for real-time assessment of rangelands. Geocarto International 7:19-26.

Everitt, J. H., and D. E. Escobar. 1996. Use of spatial information technologies for noxious plant detection and distribution on rangelands. Geocarto International 11:63-80.

Everitt, J. H., D. E. Escobar, M. A. Alaniz, and M. R. Davis. 1991. Light reflectance characteristics and video remote sensing of pricklypear. Journal of Range Management 44:587-592.

Everitt, J. H., D. E. Escobar, M. A. Alaniz, M. R. Davis, and J. V. Richerson. 1996. Using spatial information technologies to map Chinese tamarisk (*Tamarix chinenis*) infestations. Weed Science 44:194-201.

Everitt, J. H., D. E. Escobar, and M. R. Davis. 1995b. Using remote sensing for detecting and mapping noxious plants. Weed Abstracts 44:639-649.

Everitt, J. H., D. E. Escobar, R. Villarreal, M. A. Alaniz, and M. R. Davis. 1993a. Canopy light reflectance and remote sensing of shin oak (*Quercus havardii*) and associated vegetation. Weed Science 41:291-297.

Everitt, J. H., D. E. Escobar, R. Villarreal, M. A. Alaniz, and M. R. Davis. 1993b. Integration of airborne video, global positioning system, and geographic information system technologies for detecting and mapping two woody legumes on rangelands. Weed Technology 7:981-987.

Everitt, J. H., R. D. Pettit, and M. A. Alaniz. 1987. Remote sensing of broom snakeweed (*Gutierrezia sarothrae*) and spiny aster (*Aster spinosa*). Weed Science 35:295-302.

Everitt, J. H., and J. V. Richerson. 1987. Canopy reflectance of seven rangeland plant species with variable leaf pubescence. Photogrammetric Engineering and Remote Sensing 53:1571-1575.

Everitt, J. H., J. V. Richerson, M. A. Alaniz, D. E. Escobar, R. Villarreal, and M. R. Davis. 1994. Light reflectance characteristics and remote sensing of Big Bend loco (*Astragalus mollisimus* var. *earlei*) and Wooten loco (*Astragalus wootonii*). Weed Science 42:115-122.

Fitzgerald, R. W., and B. G. Lees. 1994. Assessing the classification accuracy of multisource remote sensing data. Remote Sensing of Environment 47:362-368.

Foody, G. M. 1988. The effects of viewing geometry on image classification. International Journal of Remote Sensing 9:1909-1915.

Foody, G. M. 1992. On the compensation for chance agreement in image classification accuracy assessment. Photogrammetric Engineering and Remote Sensing 58:1459-1460.

Fuentes, D. A., J. A. Gamon, H. Qiu, D. Sims, and D. A. Roberts. 2000. Mapping vegetation cover types in the Canadian boreal forest using pigment and water absorption features derived from AVIRIS. R. O. Green, editor. 2000 AVIRIS Airborne Geoscience Workshop, Pasadena, CA.

Gates, D. M., H. J. Keegan, J. C. Schleter, and V. R. Weidner. 1965. Spectral properties of plants. Applied Optics 4:11-20.

Gausman, H. W. 1977. Reflectance of leaf components. Remote Sensing of Environment 6:1-9.

Gould, W. 2000. Remote sensing of vegetation, plant species richness, and regional biodiversity hotspots. Ecological Applications 10:1861-1870.

Graetz, R. D. 1989. Remote Sensing of Terrestrial Ecosystem Structure: An Ecologist's Pragmatic View. Pages 5-30 *in* R. J. Hobbs and H. A. Mooney, editors. Remote Sensing of Biosphere Functioning. Springer-Verlag, New York, NY.

Graetz, R. D., and M. R. Gentle. 1982. The relationship between reflectance in the Landsat wavebands and the composition of an Australian semi-arid shrub rangeland. Photogrammetric Engineering and Remote Sensing 48:1721-1730.

Hansen, M., R. Dubayah, and R. Defries. 1996. Classification trees: An alternative to traditional land cover classifiers. International Journal of Remote Sensing 17:1075-1081.

Herron, G. J., R. L. Sheley, B. D. Maxwell, and J. S. Jacobsen. 2001. Influence of nutrient availability on the interaction between spotted knapweed and bluebunch wheatgrass. Restoration Ecology 9:326-331.

Hobbs, R. J. 1989. Remote sensing of spatial and temporal dynamics of vegetation. Pages 203-219 *in* R. J. Hobbs and H. A. Mooney, editors. Remote Sensing of Biosphere Functioning. Springer-Verlag, New York, NY.

Holben, B., and D. S. Kimes. 1986. Directional reflectance response in AVHRR red and near-IR bands for three cover types and varying atmospheric conditions. Remote Sensing of Environment 19:213-236.

Hudson, W. D., and C. W. Ramm. 1987. Correct formulation of the Kappa coefficient of agreement. Photogrammetric Engineering and Remote Sensing 53:421-422.

Huete, A. R., G. Hua, J. Qi, A. Chehbouni, and W. J. D. van Leeuwen. 1992. Normalization of multidirectional red and NIR reflectances with the SAVI. Remote Sensing of Environment 41:143-154.

Ioka, M., and M. Koda. 1986. Performance of Landsat-5 TM data in land-cover classfication. International Journal of Remote Sensing 7:1715-1728.

Irons, J. R., B. L. Johnson, and G. H. Linebaugh. 1986. Multiple-angle observations of reflectance anisotropy from an airborne linear array sensor. IEEE Transactions on Geoscience and Remote Sensing 25:372-383.

Irons, J. R., B. L. Markham, R. F. Nelson, D. L. Toll, D. L. Williams, R. S. Latty, and M. L. Stauffer. 1985. The effects of spatial resolution on the classification of Thematic Mapper data. International Journal of Remote Sensing 6:1385-1403.

Jackson, R. D., P. M. Teillet, and P. N. Slater. 1990. Bidirectional measurements of surface reflectance for view angle corrections of oblique imagery. Remote Sensing of Environment 32:189-202.

Janssen, L. L. F., and F. J. M. van der Wel. 1994. Accuracy assessment of satellite derived land-cover data: A review. Photogrammetric Engineering and Remote Sensing 60:419-426.

Jensen, J. R. 1996. Introductory Digital Image Processing: A Remote Sensing Perspective, Second edition. Prentice-Hall, Inc., Upper Saddle River, NJ. 318 pp.

Johnson, D. E. 1999. Surveying, mapping, and monitoring noxious weeds on rangelands. Pages 19-35 *in* R. L. Sheley and J. K. Petroff, editors. Biology and Management of Noxious Rangeland Weeds. Oregon State University Press, Coravallis, OR.

Kennedy, E. R., W. B. Cohen, and G. Takao. 1997. Empirical methods to compensate for a view-angle-dependent brightness gradient in AVIRIS imagery. Remote Sensing of Environment 62:277-291.

Kimes, D. S., and J. A. Kirchner. 1982. Radiative transfer model for heterogeneous 3-D scenes. IEEE Transactions on Geoscience and Remote Sensing 21:4119-4129.

Kimes, D. S., W. W. Newcomb, R. F. Nelson, and J. B. Schutt. 1986. Directional reflectance distribution of a hardwood and pine forest canopy. IEEE Transactions on Geoscience and Remote Sensing 24:281-293.

King, D. 1991. Determination and reduction of cover type brightness variations with view angle in airborne multispectral video imagery. Photogrammetric Engineering and Remote Sensing 57:1571-1577.

Knipling, E. B. 1970. Physical and physiological basis for the reflectance of visible and near-infrared radiation from vegetation. Remote Sensing of Environment 1:155-159.

Kreibel, K. T. 1978. Measured spectral bidirectional reflectance properties of four vegetated surfaces. Applied Optics 21:3766-3774.

Kruse, F. A. 1988. Use of airborne image spectrometer data to map minerals associated with hydrothermally altered rocks in the northern Grapevine Mountains, Nevada, and California. Remote Sensing of Environment 24:31-51.

Kruse, F. A., J. W. Boardman, and J. F. Huntington. 1999. Fifteen years of hyperspectral data: Northern Grapevine Mountains, Nevada. Eighth JPL Airborne EarthScience Workshop, Pasadena USA.

Lacey, J. R., C. B. Marlow, and J. R. Lane. 1989. Influence of spotted knapweed (*Centaurea maculosa*) on surface water runoff and sedimentation yield. Weed Technology 3:627-631.

Lajeunesse, S., R. L. Sheley, C. Duncan, and R. G. Lym. 1999. Leafy Spurge. Pages 249-260 *in* R. L. Sheley and J. K. Petroff, editors. Biology and Management of Noxious Rangeland Weeds. Oregon State University Press, Corvallis, OR.

Lass, L. W., and R. H. Callihan. 1997. The effect of phenological stage on detectibility of yellow hawkweed (*Hieracium pratense*) and oxeye daisy (*Chrysanthemum leucanthemum*) with remote multispectral digital imagery. Weed Technology 11:248-256.

Lass, L. W., H. W. Carson, and R. H. Callihan. 1996. Detection of yellow starthistle (*Centaurea solstitialis*) and common St. Johnswort (*Hypericum perforatum*) with multispectral digital imagery. Weed Technology 10:466-474.

Lauver, C. L. 1997. Mapping species diversity patterns in the Kansas shortgrass region by integrating remote sensing and vegetation analysis. Journal of Vegetation Science 8:387-394.

Lawrence, R. L., and M. P. Labus. In press. Early detection of Douglas-fir beetle infestation with sub-canopy resolution hyperspectral imagery. Western Journal of Applied Forestry.

Lawrence, R. L., and W. J. Ripple. 2000. Fifteen years of revegetation of Mount St. Helens: A landscape-scale analysis. Ecology 81:2742-2752.

Lawrence, R. L., and A. Wright. 2001. Rule-based classification systems using classification and regression tree (CART) analysis. Photogrammetric Engineering and Remote Sensing 67:1137-1142.

Lees, B. G., and K. Ritman. 1991. Decision-tree and rule-induction approach to integration of remotely sensed and GIS data in mapping vegetation in disturbed or hilly environments. Environmental Management 15:823-831.

Lefsky, M. A., W. B. Cohen, and T. A. Spies. 2001. An evaluation of alternate remote sensing products for forest inventory, monitoring, and mapping of Douglas-fir forests in western Oregon. Canadian Journal of Forest Resources 31:78-87.

Lewis, M. M. 1998. Numeric classification as an aid to spectral mapping of vegetation communities. Plant Ecology 136:133-149.

Lillesand, T. M., and R. W. Kiefer. 2000. Remote Sensing and Image Interpretation, Fourth edition. John Wiley and Sons, Inc., New York, NY. 724 pp.

Ma, Z., and R. L. Redmond. 1995. Tau coefficients for accuracy assessment of classification of remote sensing data. Photogrammetric Engineering and Remote Sensing 61:435-439.

Marshall, G. 1996. Characterizing accuracy of Trimble Pathfinder mapping receivers. Trimble Surveying and Mapping User Conference and Exposition, San Jose, CA.

Martin, M. E., S. D. Newman, J. D. Aber, and R. G. Congalton. 1998. Determining forest species composition using high spectral resolution remote sensing data. Remote Sensing of Environment 65:249-254.

Moody, M. E., and R. N. Mack. 1988. Controlling the spread of plant invasions: The importance of nascent foci. Journal of Applied Ecology 25:1009-1021.

Mouginis-Mark, P. J., H. Garbeil, and P. Flament. 1994. Effects of viewing geometry on AVHRR observations of volcanic thermal anomalies. Remote Sensing of Environment 48:51-60.

Mullin, B. 2000. State Weed Coordinator, Montana Department of Agriculture. Personal Communication, Helena, MT.

Myneni, R. B., G. Asrar, and F. G. Hall. 1992. A three-dimensional radiative transfer method for optical remote sensing of vegetated land surfaces. Remote Sensing of Environment 41:105-121.

Neale, C. M. 1997. Classification and mapping of riparian systems using airborne multispectral videography. Restoration Ecology 5:103-112.

Norman, J. M., J. M. Welles, and E. A. Walter. 1985. Contrasts among bidirectional reflectance of leaves, canopies, and soils. IEEE Transactions on Geoscience and Remote Sensing 23:659-667.

North, P. R. J. 1996. Three-dimensional forest light interaction model using a Monte Carlo method. IEEE Transactions on Geoscience and Remote Sensing 37:987-999.

Okin, G. S., D. A. Roberts, B. Murray, and W. J. Okin. 2001. Practical limits on hyperspectral vegetation discrimination in arid and semiarid environments. Remote Sensing of Environment 77:212-225.

O'Neill, M., S. L. Ustin, S. Hager, and R. Root. 2000. Mapping the distribution of leafy spurge at Theodore Roosevelt National Park using AVIRIS. R. O. Green, editor. 2000 AVIRIS Airborne Geoscience Workshop, Pasadena, CA.

O'Neill, R. V., C. T. Hunsaker, B. Jones, K. H. Riitters, J. D. Wickham, P. M. Schwartz, I. A. Goodman, B. L. Jackson, and W. S. Baillargeon. 1997. Monitoring environmental quality at the landscape scale. Bioscience 47:513-519.

Peters, A. J., B. C. Reed, M. D. Eve, and K. C. McDaniel. 1992. Remote sensing of broom snakeweed (*Gutierrezia sarothrae*) with NOAA-10 spectral image processing. Weed Technology 6:1015-1020.

Phinn, S. R., J. Franklin, A. Hope, D. A. Stow, and L. Huenneke. 1996. Biomass distributions using airborne digital video imagery and spatial statistics in a semi-arid environment. Journal of Environmental Management 47:139-164.

Phinn, S. R., D. A. Stow, and D. Van Mouwerik. 1999. Remotely sensed estimates of vegetation structural characteristics in restored wetlands, southern California. Photogrammetric Engineering and Remote Sensing 65:485-493.

Pickup, G., V. H. Chewings, and G. Pearce. 1995. Procedures for correcting high resolution airborne video imagery. International Journal of Remote Sensing 16:1647-1662.

Pitts, D. E., and G. Badhwar. 1980. Field size, length, and width distributions based on LACIE ground truth data. Remote Sensing of Environment 10:201-213.

Pons, X., and L. Sole-Sugraines. 1994. A simple radiometric correction model to improve automatic mapping of vegetation from multispectral satellite data. Remote Sensing of Environment 48:191-204.

Price, J. C. 1994. How unique are spectral signatures? Remote Sensing of Environment 49:181-186.

Price, J. C. 1997. Spectral band selection for visible-near infrared remote sensing: spectral-spatial resolution tradeoffs. IEEE Transactions on Geoscience and Remote Sensing 35:1277-1285.

Price, K. P., T. J. Crooks, and E. A. Martinko. 2001. Grasslands across time and scale: A remote sensing perspective. Photogrammetric Engineering and Remote Sensing 67:414-420.

Qi, J., A. R. Huete, F. Cabot, and A. Chebhouni. 1994. Bidirectional properties and utilization of high resolution spectra from a semi-arid watershed. Water Resources Research 30:1271-1279.

Qi, J., M. S. Moran, F. Cabot, and G. Dedieu. 1995. Normalization of sun/view angle effects using spectral albedo-based vegetation indices. Remote Sensing of Environment 52:207-217.

Ramsey, E. W., G. A. Nelson, S. K. Sapkota, E. B. Seeger, and K. D. Martella. 2002. Mapping Chinese tallow with color-infrared photography. Photogrammetric Engineering and Remote Sensing 68:251-255.

Ranson, K. J., J. R. Irons, and C. S. T. Daughtry. 1991. Surface albedo form bidirectional reflectance. Remote Sensing of Environment 35:201-211.

Roberts, D. A., M. Gardner, R. Church, S. L. Ustin, G. Scheer, and R. O. Green. 1998. Mapping chaparral in the Santa Monica Mountains using multiple endmember spectral mixture models. Remote Sensing of Environment 65:267-279.

Roberts, D. A., M. O. Smith, and J. B. Adams. 1993. Green vegetation, nonphotosynthetic vegetation, and soils in AVIRIS data. Remote Sensing of Environment 44:255-269.

Root, R., S. Hager, G. L. Anderson, S. L. Ustin, L. Costick, J. Smith, and R. O. Green. 2001. Detection and mapping of leafy spurge at Theodore Roosevelt National Park and vicinity using AVIRIS hyperspectral imaging. http://biology.usgs.gov/hwsc/leafproj.htm.

Rosenfield, G. H., and K. Fitzpatrick-Lins. 1986. A coefficient of agreement as a measure of thematic classification accuracy. Photogrammetric Engineering and Remote Sensing 52:223-227.

Royer, A., P. Vincent, and F. Bonn. 1985. Evaluation and correction of viewing angle effects on satellite measurements of bidirectional reflectance. Photogrammetric Engineering and Remote Sensing 51:1899-1914.

Sandmeier, S., C. Muller, B. Hosgood, and G. Andreoli. 1998. Physical mechanisms in hyperspectral BRDF data of grass and watercress. Remote Sensing of Environment 66:222-233.

Schaaf, C. B., and A. H. Strahler. 1994. Validation of bidirectional and hemispherical reflectances from a geometric-optical model using ASAS imagery and Pyranometer measurements of a spruce forest. Remote Sensing of Environment 49:138-144.

Sheley, R. L., J. S. Jacobs, and M. F. Carpinelli. 1998. Distribution, biology, and management of diffuse knapweed (*Centaurea diffusa*) and spotted knapweed (*Centaurea maculosa*). Weed Technology 99:353-362.

Sheley, R. L., J. S. Jacobs, and M. F. Carpinelli. 1999a. Spotted Knapweed. Pages 350-361 *in* R. L. Sheley and J. K. Petroff, editors. Biology and Management of Noxious Rangeland Weeds. Oregon State University Press, Corvallis, OR.

Sheley, R. L., S. Kedzie-Webb, and B. D. Maxwell. 1999b. Integrated weed management on rangeland. Pages 57-68 *in* R. L. Sheley and J. K. Petroff, editors. Biology and Management of Noxious Rangeland Weeds. Oregon State University Press, Corvallis, OR.

Sheley, R. L., L. L. Larson, and D. E. Johnson. 1993. Germination and root dynamics of range weeds and forage species. Weed Technology 7:234-237.

Sheley, R. L., T. J. Svejcar, and B. D. Maxwell. 1996. A theoretical framework for developing successional weed management strategies on rangeland. Weed Technology 10:766-773.

Smith, M. O., S. L. Ustin, J. B. Adams, and A. R. Gillespie. 1990. Vegetation in deserts: I. A regional measure of abundance from multispectral images. Remote Sensing of Environment 31:1-26.

Sohn, Y., and R. M. McCoy. 1997. Mapping desert shrub rangeland using spectral unmixing and modeling spectral mixtures with TM data. Photogrammetric Engineering and Remote Sensing 63:707-716.

Stehman, S. V. 1997. Selecting and interpreting measures of thematic classification accuracy. Remote Sensing of Environment 62:77-89.

Stehman, S. V. 2001. Statistical rigor and practical utility in thematic map accuracy assessment. Photogrammetric Engineering and Remote Sensing 67:727-734.

Stehman, S. V., and R. L. Czaplewski. 1998. Design and analysis for thematic accuracy assessment: Fundamental principles. Remote Sensing of Environment 64:331-344.

Story, M., and R. G. Congalton. 1986. Accuracy assessment: A user's perspective. Photogrammetric Engineering and Remote Sensing 52:397-399.

Townshend, J. R. G. 1980. The spatial resolving power of earth resources satellites: A review. NASA Goddard Space Flight Center, Greenbelt, MD.

Townshend, J. R. G., and C. O. Justice. 1981. Information extraction from remotely sensed data. International Journal of Remote Sensing 2:313-329.

Treitz, P. M., P. J. Howarth, and R. C. Suffling. 1992. Application of detailed ground information to vegetation mapping with high spatial resolution imagery. Remote Sensing of Environment 42:65-82.

Tucker, C. J., J. R. G. Townshend, and T. E. Goff. 1985. African land-cover classification using satellite data. Science 227:369-375.

Tueller, P. T. 1989. Remote sensing technology for rangeland management applications. Journal of Range Management 42:442-453.

Tyser, R. W., and C. H. Key. 1988. Spotted knapweed in natural area fescue grasslands: an ecological assessment. Northwest Science 62:151-160.

USGS. 2001. Map Accuracy Standards: Digital Orthophoto Quadrangles. USGS Fact Sheet 057-01, United States Geological Service, Reston, VA.

Ustin, S. L., Q. J. Hart, L. Duan, and G. Scheer. 1996. Vegetation mapping on hardwood rangelands in California. International Journal of Remote Sensing 17:3015-3036.

Ustin, S. L., and Q. F. Xiao. 2001. Mapping successional boreal forests in interior central Alaska. International Journal of Remote Sensing 22:1779-1797.

Venables, W. N., and B. D. Ripley. 1997. Modern Applied Statistics with S-Plus, Second edition. Springer-Verlag, New York, NY. 548 pp.

Vitousek, P. M., C. M. D'Antonio, L. L. Loope, and R. Westbrooks. 1996. Biological invasions as global environmental change. American Scientist 84:468-478.

Walsh, S. J. 1987. Variability of Landsat MSS spectral responses of forests in relation to stand and site characteristics. International Journal of Remote Sensing 8:1289-1299.

Walthall, C. L. 1997. A study of reflectance anisotropy and canopy structure using a simple empirical model. Remote Sensing of Environment 61:118-128.

Walthall, C. L., J. M. Norman, J. M. Welles, G. C. Campbell, and B. L. Blad. 1985. Simple equation to approximate the bidirectional reflectance of vegetation and soil surfaces. Applied Optics 24:383-387.

Wessman, C. A., C. A. Bateson, and T. L. Benning. 1997. Detecting fire and grazing patterns in tallgrass prairie using spectral mixture analysis. Ecological Applications 7:493-511.

Williams, D. L., J. R. Irons, B. L. Markham, R. F. Nelson, D. L. Toll, R. S. Latty, and M. L. Stauffer. 1984. A statistical evaluation of the advantages of Landsat Thematic Mapper data in comparison to Multispectral Scanner data. IEEE Transactions on Geoscience and Remote Sensing 22:294-302.

Woodcock, C. E., and A. H. Strahler. 1987. The factor of scale in remote sensing. Remote Sensing of Environment 21:311-332.

Woolley, J. T. 1971. Reflectance and transmittance of light by leaves. Plant Physiology 47:656-662.

Wylie, B. K., D. J. Meyer, M. J. Choate, L. Vierling, and P. K. Kozak. 2000. Mapping woody vegetation and eastern red cedar in the Nebraska Sand Hills using AVIRIS. R. O. Green, editor. 2000 AVIRIS Airborne Geoscience Workshop, Pasadena, CA.

Zamora, D. L., and D. C. Thill. 1999. Early detection and eradication of new weed infestations. Pages 73-84 *in* R. L. Sheley and J. K. Petroff, editors. Biology and Management of Noxious Rangeland Weeds. Oregon State University Press, Corvallis, OR.

APPENDICES

APPENDIX A

SPECTRAL ANGLE MAPPER (SAM) CLASSIFICATION OF HYPERSPECTRAL IMAGERY

In addition to the CART analysis, we applied ENVI's SAM algorithm to the hyperspectral imagery. The results of the SAM classifications were compared to CART classifications for each site. In this case, sensor, spatial resolution, and spectral resolution were held constant while the classification algorithm varied. As a result, the Khats from the SAM and CART classifications were used in a two-tailed Z test to determine if there were statistically significant differences between the algorithms applied to the same imagery (Congalton and Green 1999). The sample variance of Kappa was computed using the Delta method (Congalton and Green 1999).

Image Processing and Analysis

Initially we applied SAM to a mosaicked scene without attempting to correct for scene illumination differences. One scene was distinctly brighter than the other four scenes and to mitigate the differences we simply dropped the disparate scene, creating a composite of the other four scenes and resampling to 5 m using the nearest neighbor function. Although modeling bidirectional reflectance and correcting illumination differences was beyond the scope of the project, we decided to test whether cross-track illumination correction (CTIC), a function incorporated into ENVI, would impact classification accuracies. We applied the CTIC to each of the four scenes before georeferencing. Before resampling we measured several transects within each scene to compute the nominal pixel size. Pixel size was less than 5 m, averaging approximately 3.5 m. Therefore, we resampled the CTIC imagery to 3 m using the nearest neighbor function. We applied the SAM algorithm to the non-CTIC, 5 m imagery and the CTIC, 3 m imagery.

SAM is a physically based process that plots spectra in n-dimensional space with n equal to the number of spectral bands (ENVI 1997). Unknown pixels were plotted as vectors in 128-dimensional space (all bands were used). The angle of an unknown vector, measured in radians, was compared to the angles of reference spectra, in our case image endmembers extracted from GPS data. SAM classified each unknown pixel based on the similarity of vector angle to the vector angle of reference spectra. Image endmembers were obtained from the GPS reference polygons. We used the software default of 0.1 radians to run the algorithm. Pixels beyond this angle were not considered similar to reference spectra and therefore not classified.

Results

Euphorbia esula

Using the strictest interpretation of accuracy for the SAM classified map, user's accuracy for *E. esula* was 53%, user's accuracy for vegetation was 73%, overall accuracy was 66%, and the Khat value was 0.26 (Table 9). The resulting map revealed that *E. esula* infestations were concentrated in drainages and nearby hillsides (Figure 6). As the thresholds became less stringent, there were slight increases until all accuracies peaked at the 50% threshold (Figure 7). At the 50% threshold, user's accuracy for *E. esula* was 58%, user's accuracy for vegetation was 73%, overall accuracy was 68%, and the Khat statistic was 0.29. Thereafter, accuracies and Khat showed little to no change until a high enough percentage threshold was reached where all vegetation polygons were correctly classified, resulting in 100% user's accuracy for *E. esula*. Comparing the Khat values of the SAM and CART error matrices resulted in no significant differences between classifications at any threshold (p-value = 0.62 at 0% threshold.

Table 9. Error matrix summary measures for (a) SAM classification of *E. esula* at 0% and 50% threshold decision rules. (b) Error matrix summary measures for Non-CTIC and CTIC SAM classification of *C. maculosa* at 0% threshold decision rule.

SAM: 0% Threshold		
%	*E. esula*	Vegetation
User's	53	73
Producer's	51	75
Overall	66	
Khat	0.26	
SAM: 50% Threshold		
%	*E. esula*	Vegetation
User's	58	73
Producer's	47	81
Overall	68	
Khat	0.29	

(a)

Non-CTIC SAM: 0% Threshold		
%	*C. maculosa*	Vegetation
User's	38	43
Producer's	37	44
Overall	40	
Khat	-0.19	
CTIC SAM: 0% Threshold		
%	*C. maculosa*	Vegetation
User's	39	42
Producer's	43	38
Overall	40	
Khat	-0.19	

(b)

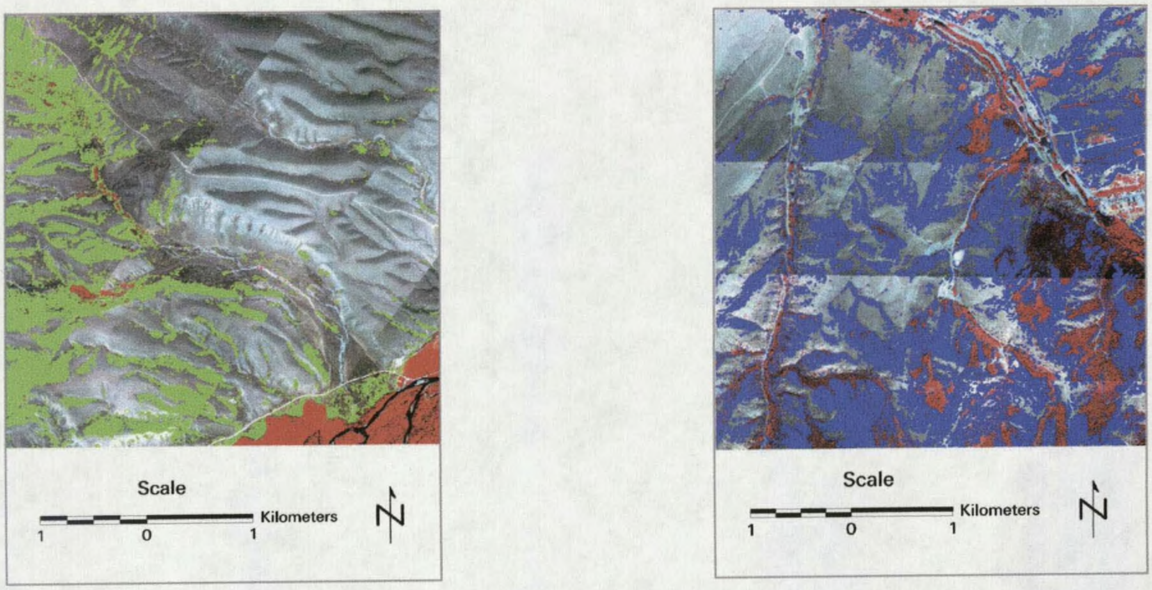

(a) (b)

Figure 6. SAM classification of (a) *E. esula* overlaid on hyperspectral imagery and (b) non-CTIC SAM classification of *C. maculosa* overlaid on hyperspectral imagery. Bands 24 (784 nm), 16 (662 nm), and 9 (555 nm) are displayed as red, green, and blue.

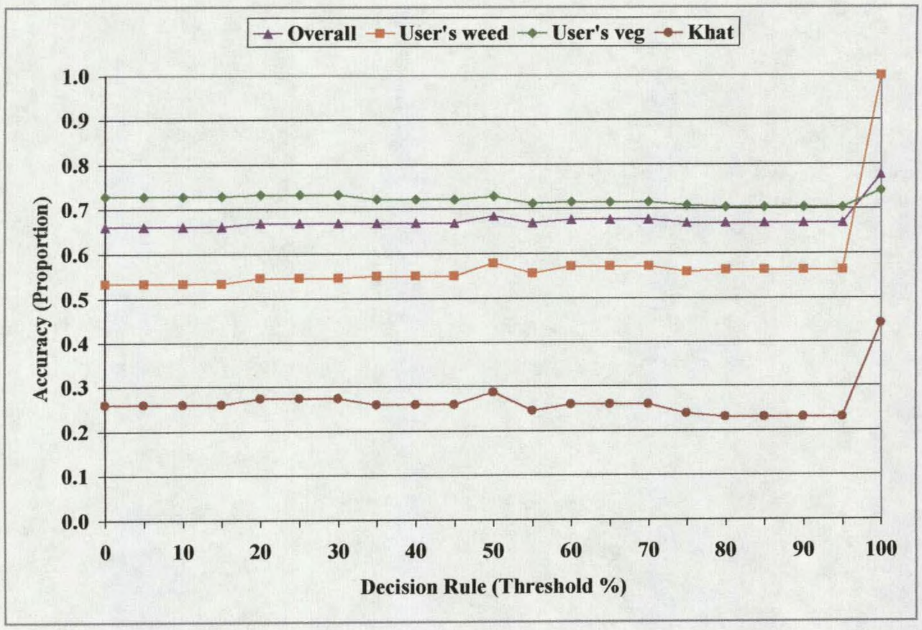

(a)

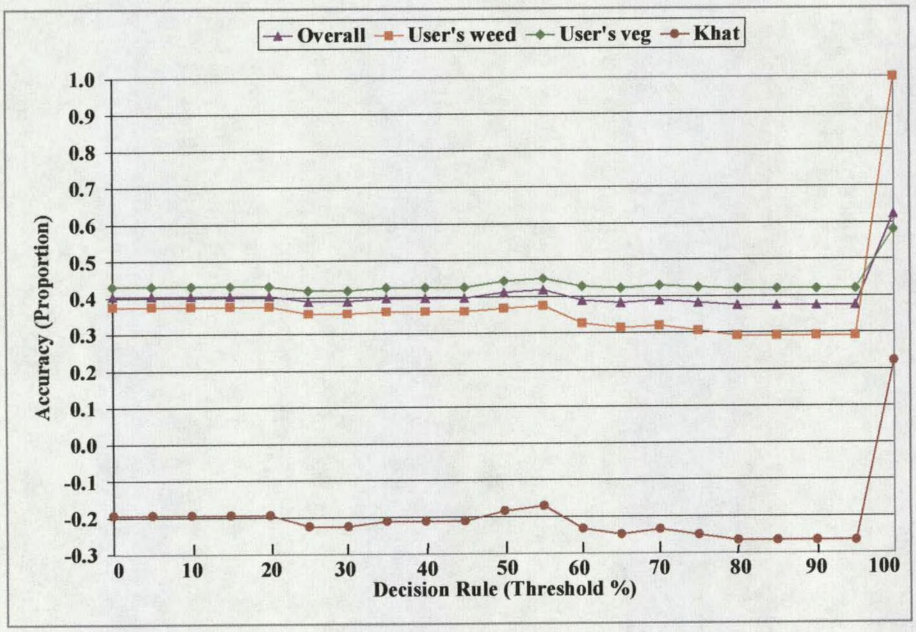

(b)

Figure 7. Accuracy assessment curves comparing incremental decision rules for (a) SAM hyperspectral classification of *E. esula* and (b) Non-CTIC SAM hyperspectral classification of *C. maculosa*.

<u>Centaurea maculosa</u>

The SAM classification of *C. maculosa* was less accurate than the SAM classification of *E. esula* and was quite poor. Using the strictest interpretation of accuracy for the SAM classified map, user's accuracy for *C. maculosa* was 38%, user's accuracy for vegetation was 43%, overall accuracy was 40%, and the Khat value was -0.19 (Table 9). A Khat value less than 0 indicates the classification is essentially no better than a random classification (Cohen 1960, Congalton and Green 1999). The resulting map revealed overclassification of *C. maculosa*, with heavy infestations mapped throughout the study area (Figure 6). The SAM algorithm was unable to distinguish *C. maculosa* from vegetation with any reliability. Accuracies showed little improvement with less strict decision rules (Figure 7). Comparing Khat values of SAM and CART error matrices resulted in significant differences at all thresholds (p-value = 0.0001 at 0% threshold).

We classified the same imagery, but processed with ENVI's CTIC function to test if illumination correction improved accuracy. The accuracies of the CTIC SAM classification were slightly different from the non-CTIC classification (Table 9). There was not a statistical difference between CTIC and non-CTIC classifications (p-value = 0.99 at 0% threshold).

Discussion

There was no statistical difference between Khats for hyperspectral imagery classified with SAM and hyperspectral imagery classified with CART for *E. esula*. Our results showed that for the given methodology, hyperspectral (SAM or CART) imagery produced statistically similar results, and a manager might base a choice of algorithm for mapping *E. esula* on cost or processing simplicity. SAM resulted in a 12% increase in weed user's accuracy over the multispectral ML classification and was 8% less than the CART classification.

SAM utilized training sample responses in all 128 spectral bands, plotting a vector through the response cloud that represented *E. esula* or vegetation training pixels. In using all spectral bands, the overlap between *E. esula* and vegetation responses might have decreased the angular difference between vectors, increasing the confusion between the classes.

For *C. maculosa*, the Khat statistics for the non-CTIC and the CTIC SAM classifications were significantly lower than the hyperspectral CART Khat statistic. However, both the hyperspectral SAM and the multispectral ML Khats were so low as to warrant the classifications unproductive. A Kappa coefficient of agreement for exactly chance agreement equals zero, with the upper limit of perfect agreement equal to 1 (Cohen 1960). Although a numerical lower limit for Kappa might be computed from the column and row marginals of an error matrix, a negative Kappa, or less than chance agreement is essentially disagreement, and the categorization "of no further practical interest" (Cohen 1960). The SAM algorithm for *C. maculosa* resulted in a random classification no better than expected from assigning pixels to categories by chance. Little practical information can be inferred from such a poor classification. There was little to no reliability of the *C. maculosa* locations derived from the SAM map, and using the methodology, we followed, the SAM algorithm is not recommended for mapping *C. maculosa*.

Established infestations of *C. maculosa* tend to outcompete native plants for limiting resources, and as a result, reduce understory and increase exposed bare soil (Herron et al. 2001). If *C. maculosa* spectra appeared very similar to vegetation spectra, except brighter due to a higher soil component, SAM would plot the two targets in very similar spectral space, although the lengths would differ because of brightness differences. Increased soil exposure and reflectance resulting from *C. maculosa* invasion might have influenced the SAM algorithm.

APPENDIX B

DETAILED SENSOR AND IMAGE INFORMATION

Multispectral Imagery

Positive Systems, Inc. (PSI) of Whitefish, MT, provided the high spatial resolution multispectral imagery. The *E. esula* site was flown on 7 August 1999 at approximately 11 am Mountain Daylight Time (MDT). Twenty-eight individual scenes were imaged to cover the study sites. The *C. maculosa* site was flown on 10 August 1999 at approximately 11 am MDT. Forty individual scenes were imaged to cover the study sites. The low flying height resulted in a nominal spatial resolution of 1 m.

To obtain the imagery, PSI used the Airborne Data Acquisition and Registration (ADAR) 5500 system, an electronic imaging instrument composed of four Kodak DCS 460 cameras each mounted with 20 mm lenses. Each digital camera used a photosensitive detector to record electromagnetic energy with a charge-coupled device (CCD) in an area array. Cameras were individually filtered to record reflectance over the ranges 460 – 550 nm, 520 – 610 nm, 610 – 700 nm, and 780 – 920 nm, centering on blue, green, red, and NIR portions of the spectrum, respectively. The CCD recorded intensity of reflected light in each filtered portion of the spectrum as brightness values quantized in 8-bit format. The four bands were coregistered by PSI to produce one multispectral image per scene containing four spectral dimensions.

Hyperspectral Imagery

Earth Search Sciences, Inc. (ESSI) of Kalispell, MT, provided the hyperspectral imagery. The *E. esula* and *C. maculosa* sites were both flown on 25 August 1999 from approximately 12 pm to 2 pm MDT. Six individual scenes were imaged to cover the *E. esula* study site and seven scenes were imaged to cover the *C. maculosa* site.

To obtain the hyperspectral imagery, ESSI used the Probe-1 sensor. The Probe-1 is a whiskbroom or across-track scanning instrument, imaging contiguous strips of ground in an along-track direction as the aircraft moves forward. The Probe-1 sensor consisted of four spectrometers that recorded incoming light in 128 bands in the VIS, NIR, and shortwave infrared (SWIR) portions of the spectrum. The bandwidth average for each spectrometer ranged from 12 - 16 nm, and these narrow channels produced a nearly continuous spectral range from 440 – 2507 nm. The brightness values are quantized in 10-bit format.

ESSI specifies for Probe-1 an instantaneous field of view of 2.5 milliradians in the along track direction, which results in a ground resolution cell of 5 m when flying at an average height above ground level of 2500 m (Earth Search Sciences 2002). Spatial resolution varies with platform altitude and scan angle and decreases with lower flying heights and increases as the instrument looks away from nadir. When averaging pixel sizes, however, we consistently found cell sizes to be less than 5 m and closer to 3.5 m.

APPENDIX C

ERROR MATRICES AND SUMMARY MEASURES

Table 10. Error matrices for multispectral ML classification of (a) *E. esula* at strict (0%) and 50% threshold decision rules and (b) *C. maculosa* at strict and 45% threshold decision rules.

0% Threshold

Classified Data	Reference Data		
	Vegetation	*E. esula*	Row Total
Vegetation	24	5	29
E. esula	61	43	104
Column Total	85	48	133

Producer's Accuracy
Vegetation = 24/85 = 28%
E. esula = 43/48 = 90%

User's Accuracy
Vegetation = 24/29 = 83%
E. esula = 43/104 = 41%

Overall Accuracy = (24+43)/133 = 50%
Khat = 0.14

50% Threshold

Classified Data	Reference Data		
	Vegetation	*E. esula*	Row Total
Vegetation	82	32	114
E. esula	3	16	19
Column Total	85	48	133

Producer's Accuracy
Vegetation =82/85 = 96%
E. esula = 16/48 = 33%

User's Accuracy
Vegetation =82/114 = 72%
E. esula = 16/19 = 84%

Overall Accuracy = (82+16)/133 = 74%
Khat = 0.34

(a)

0% Threshold

Classified Data	Reference Data		
	Vegetation	*C. maculosa*	Row Total
Vegetation	11	4	15
C. maculosa	77	64	141
Column Total	88	68	156

Producer's Accuracy
Vegetation = 11/88 = 13%
C. maculosa = 64/68 = 94%

User's Accuracy
Vegetation = 11/15 = 73%
C. maculosa = 64/141 = 45%

Overall Accuracy = (11+64)/156 = 48%
Khat = 0.06

45% Threshold

Classified Data	Reference Data		
	Vegetation	*C. maculosa*	Row Total
Vegetation	73	35	108
C. maculosa	15	33	48
Column Total	88	68	156

Producer's Accuracy
Vegetation = 73/88 = 83%
C. maculosa = 33/68 = 49%

User's Accuracy
Vegetation = 73/108 = 68%
C. maculosa = 33/48 = 69%

Overall Accuracy = (73+33)/156 = 68%
Khat = 0.33

(b)

Table 11. Error matrices for hyperspectral CART classification of (a) *E. esula* at strict and 50% threshold decision rules and (b) *C. maculosa* at strict and 25% threshold decision rules.

CART 0% Threshold

Classified Data	Reference Data		
	Vegetation	*E. esula*	Row Total
Vegetation	68	24	92
E. esula	15	23	38
Column Total	83	47	130

Producer's Accuracy
Vegetation = 68/83 = 82%
E. esula = 23/47 = 49%

User's Accuracy
Vegetation = 68/92 = 74%
E. esula = 23/38 = 61%

Overall Accuracy = (68+23)/130 = 70%
Khat = 0.32

CART 50% Threshold

Classified Data	Reference Data		
	Vegetation	*E. esula*	Row Total
Vegetation	79	29	108
E. esula	4	18	22
Column Total	83	47	130

Producer's Accuracy
Vegetation =79/83 = 95%
E. esula = 18/47 = 38%

User's Accuracy
Vegetation = 79/108 = 73%
E. esula = 18/22 =82%

Overall Accuracy = (79+18)/130 = 75%
Khat = 0.38

(a)

CART 0% Threshold

Classified Data	Reference Data		
	Vegetation	*C. maculosa*	Row Total
Vegetation	64	40	104
C. maculosa	10	28	38
Column Total	74	68	142

Producer's Accuracy
Vegetation = 64/74 = 86%
C. maculosa = 28/68 = 41%

User's Accuracy
Vegetation = 64/104 = 62%
C. maculosa = 28/38 = 74%

Overall Accuracy = (64+28)/142 = 65%
Khat = 0.28

CART 25% Threshold

Classified Data	Reference Data		
	Vegetation	*C. maculosa*	Row Total
Vegetation	70	43	113
C. maculosa	4	25	29
Column Total	74	68	142

Producer's Accuracy
Vegetation = 64/74 = 95%
C. maculosa =25/68 = 37%

User's Accuracy
Vegetation = 70/113 = 62%
C. maculosa = 25/29 = 86%

Overall Accuracy = (70+25)/142 =67%
Khat = 0.32

(b)

Table 12. Error matrices for hyperspectral SAM classification of (a) *E. esula* at strict and 50% threshold decision rules and (b) *C. maculosa* at strict threshold decision rule.

SAM 0% Threshold

Classified Data	Reference Data		
	Vegetation	*E. esula*	Row Total
Vegetation	62	23	85
E. esula	21	24	45
Column Total	83	47	130

Producer's Accuracy
Vegetation = 62/83 = 75%
E. esula = 24/47 = 51%

User's Accuracy
Vegetation = 62/85 = 73%
E. esula = 24/45 = 53%

Overall Accuracy = (62+24)/130 = 66%
Khat = 0.26

SAM 50% Threshold

Classified Data	Reference Data		
	Vegetation	*E. esula*	Row Total
Vegetation	67	25	92
E. esula	16	22	38
Column Total	83	47	130

Producer's Accuracy
Vegetation = 67/83 = 81%
E. esula = 22/47 = 47%

User's Accuracy
Vegetation = 67/92 = 73%
E. esula = 22/38 = 58%

Overall Accuracy = (67+22)/130 = 68%
Khat = 0.29

(a)

SAM 0% Threshold

Classified Data	Reference Data		
	Vegetation	*C. maculosa*	Row Total
Vegetation	31	41	72
C. maculosa	40	24	64
Column Total	71	65	136

Producer's Accuracy
Vegetation = 31/71 = 44%
C. maculosa = 24/65 = 37%

User's Accuracy
Vegetation = 31/72 = 43%
C. maculosa = 24/64 = 38%

Overall Accuracy = (31+24)/136 = 40%
Khat = -0.19

(b)

APPENDIX D

CLASSIFICATION AND REGRESSION TREE (CART) DIAGRAMS

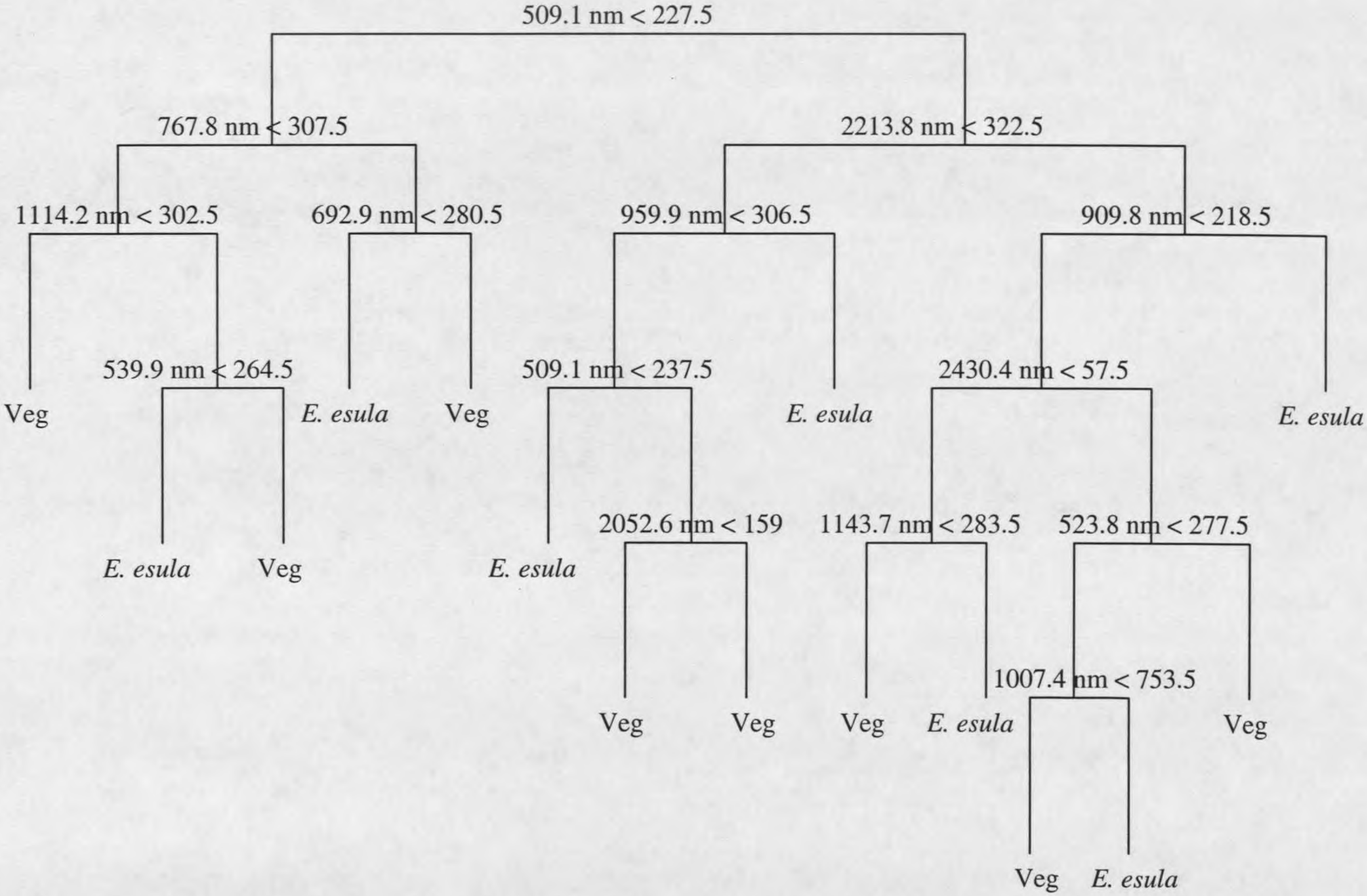

Figure 8. CART diagram showing hierarchical splits for *E. esula* and associated vegetation

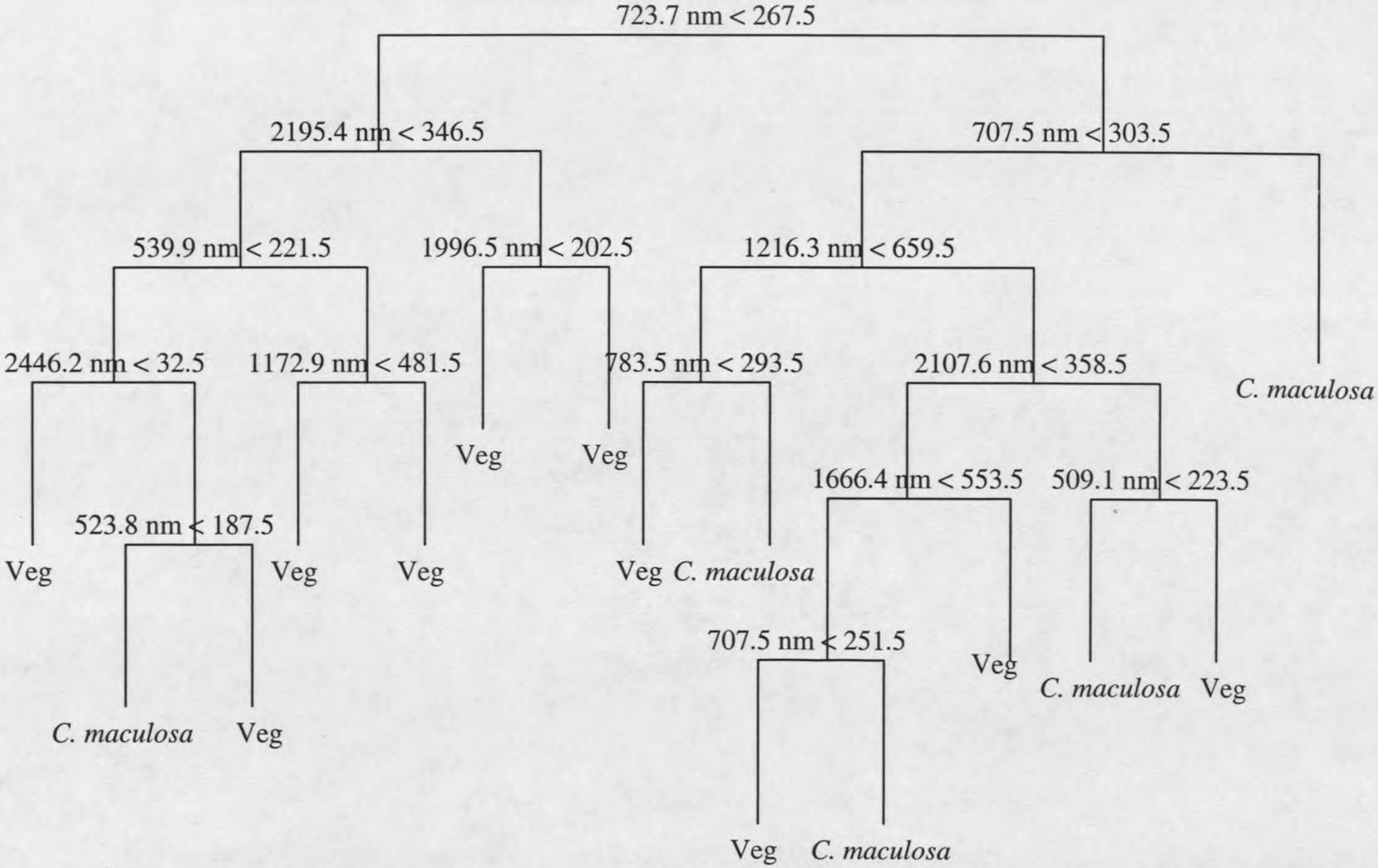

Figure 9. CART diagram showing hierarchical splits for *C. maculosa* and associated vegetation

APPENDIX E

EXAMPLE MAP OF REFERENCE SAMPLE DISTRIBUTIONS

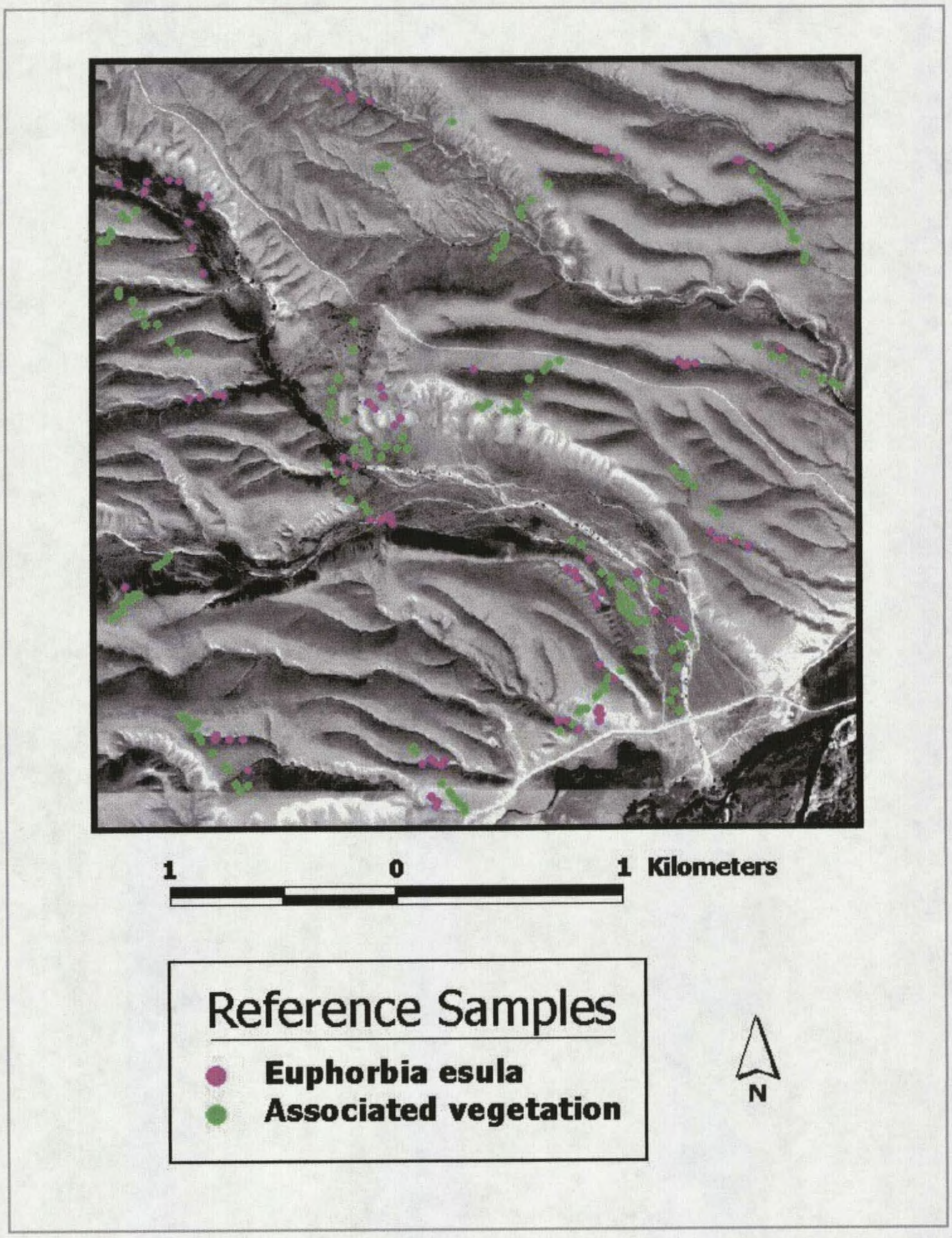

Figure 10. Map of reference samples of target weed and associated vegetation for *E. esula* site overlaid on DOQ.